

ConDA: Unsupervised Domain Adaptation for LiDAR Segmentation via Regularized Domain Concatenation

Lingdong Kong^{1,*}, Niamul Quader², Venice Erin Liong², and Hanwang Zhang¹

¹ Nanyang Technological University

² Motional

lingdong001@e.ntu.edu.sg, niamul.quader@motional.com,
venice.liong@motional.com, hanwangzhang@ntu.edu.sg

Abstract. Transferring knowledge learned from the labeled source domain to the raw target domain for unsupervised domain adaptation (UDA) is essential to the scalable deployment of an autonomous driving system. State-of-the-art methods in UDA often employ a key idea: utilizing joint supervision signals from both of the source domain (with ground-truth) and target domain (with pseudo-labels) for self-training. In this work, we improve and extend on this aspect. We present **ConDA**, a **C**oncatenation-based **D**omain **A**daptation framework for LiDAR segmentation that: 1) constructs an intermediate domain consisting of fine-grained interchange signals from both source and target domains without destabilizing the semantic coherency of objects and background around the ego-vehicle; and 2) utilizes the intermediate domain for self-training. To improve both the network training on the source domain and self-training on the intermediate domain, we propose an anti-aliasing regularizer and an entropy aggregator to reduce the negative effect caused by the aliasing artifacts and noisy pseudo labels. Through extensive experiments, we demonstrate that ConDA significantly outperforms prior arts in mitigating the domain gap not only in UDA, but also in other DAs with minimum supervisions, such as semi-/weakly-supervised DAs. Code will be publicly available³.

Keywords: Domain Adaptation · Scene Mapping · LiDAR Perception

1 Introduction

Large-scale annotated data are always desirable as they often yield robust and generalizable models. However, annotating semantic labels for 3D data like LiDAR point clouds [37] in autonomous driving [7,19,5,30,66,9,25] is extremely expensive [90,24]. This motivates us to explore unsupervised domain adaptation (UDA) for transferring knowledge [51] learned from one domain, *e.g.*, Boston, to another one, *e.g.*, Singapore, for scalable cross-city⁴ deployment.

* Work done as an autonomous vehicle intern at Motional.

³ <https://github.com/ldkong1205/ConDA>.

⁴ Particularly related to mapping areas that autonomous vehicles have not seen before.

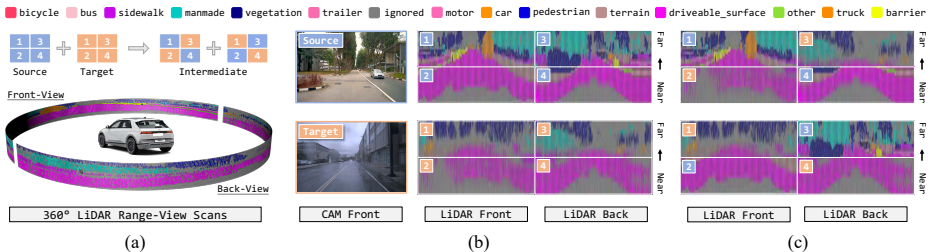


Fig. 1. Illustrative examples for domain concatenation. (a) Cylindrical representation of LiDAR range-view (RV); Stripes 1 and 2 corresponds to the front-view while 3 and 4 are the back-view of the ego-vehicle. (b) Visual RGB and LiDAR RV projections of the *source* (ground-truth) and *target* (pseudo-labels) domains. Samples adopted from nuScenes [7]. (c) Concatenated examples. Mixing domains using our ConDA strategy yields semantically realistic intermediate domain samples for self-training.

UDA aims to tackle scenarios where a model is trained on labeled data from a *source* domain and unlabeled data from a different but related *target* domain, with the goal of enabling the model to perform well during target test time. A common practice in UDA is to jointly learn from both of the source and target domains [69]. Prior works fall into the following two lines: 1) implicit learning domain-invariant features with domain discriminators via adversarial training [22,26,23], and 2) self-training with joint supervision signals from both the source (with ground-truth) and target (with pseudo-labels generated by confidence thresholding) domains [36,98]. Recent studies have shown that the latter often yields more robust models with less computation cost [100,4]. These works, however, learn separately from source and target batches, and thus lack of learning fine-grained interactions of objects and background in-between domains.

Implementing an intermediate domain that can facilitate interactions to reduce the domain gap is intuitive. The ground-truth signals from the source domain can construct a “shortcut” for correcting false target predictions in the local vicinity since feature representations close to each other tend to have the same semantic label [42]. Additionally, the target “pseudo supervisions” – which often contain large amounts of ignored labels – can serve as a strong consistency regularization [20] for the source domain. This guided supervision and regularization may yield a more adaptable and robust feature learning. It is not easy, however, to directly mix domains via interpolation [92,74,6] or superposition [91,15] for semantic segmentation as such techniques can corrupt the semantic coherency [20] of the intermediate domain.

Concatenating Domains. In this work, we propose a concatenation-based domain adaptation (ConDA) approach for cross-city UDA in LiDAR segmentation. ConDA enables the interactions of fine-grained semantic information in-between the source and target cities (domains) while not destabilizing the semantic coherency. We make the observations that although the overall distributions for the source and target domains are very different, there is a strong likelihood that similar objects and background tend to occupy particular regions in the

LiDAR range-view (RV) around the ego-vehicle (*cf.* Fig. 1a). As an example, the bottom-half views of both source and target domains are mostly composed of ‘driveable surface’, whereas the upper-half views tend to contain ‘barrier’, ‘car’, ‘vegetation’, etc. (*cf.* Fig. 1b). We exploit this important correlation to construct the ConDA intermediate domain that selects non-overlapping regions of point clouds from both source and target domains and concatenates them together, while maintaining the relative positions from the ego-vehicle. As shown in Fig. 1c, concatenating different regions (*e.g.*, front-top, front-bottom, back-top, and back-bottom) of RV stripes from different domains can still preserve semantic consistency. We will revisit this formally in Sec. 3.2.

The proposed domain concatenation strategy provides a better solution for model self-training via interchanged supervisions from both the source domain and the target domain. It is worth noting that the quality of the pseudo-labels – and in turn the generalizability of the initial training on the source domain – becomes essential since erroneous “pseudo supervision” can do evil in self-training. We counter this problem from two perspectives as follows.

Aliasing Suppression. First, the generalizability of the model can be improved by removing high-frequency noisy aliasing artifacts [73,93] with careful placements of low-pass anti-aliasing filters [99]. However, empirically designing such filters is challenging in the context of UDA, since the lack of target domain ground-truth prevents any empirical experiments. To reduce the detrimental effect of high-frequency aliasing artifacts [63,8] without accessing target annotations, we propose a built-in regularization mechanism (*cf.* Sec. 3.3) within each convolution block to regularize high-frequency representation learning during training, as well as to mitigate possible aliasing caused by region re-grouping.

Entropy Aggregation. Furthermore, as the pseudo-labels are “guessed” by the model trained on the source domain, it is intuitive to leverage the uncertainty [27] of such “guesses” for filtering non-confident selections. Entropy [62] – a measure of choice freedom – has been proven conducive in recent works for estimating prediction uncertainty [97,78]. Different from prior arts that implicitly minimize entropy in an adversarial way [75,50], we design an entropy aggregator (*cf.* Sec. 3.4) which explicitly eliminates high entropy target predictions and thus improves the overall quality for the intermediate domain supervisions.

Overall, this work has the following key contributions:

- We propose ConDA, a novel framework that facilitates fine-grained interactive learning in-between the source and target domains. To the best of our knowledge, we are the first work that explored cross-city UDA for uni-modal LiDAR segmentation, which can serve as a baseline for future research.
- We design two regularization techniques to reduce detrimental aliasing artifacts and uncertain target predictions during pre-training and self-training.
- We conduct comprehensive studies on the effects of our technical contributions on challenging UDA scenarios with nuScenes [7]. Our methods provide significant performance gains over state-of-the-art approaches.
- ConDA is a generic knowledge transfer design, hence it can be deployed in other DA settings under annotation scarcity (with semi/weak supervisions).

2 Related Work

UDA on Visual RGB. Adversarial training [22,23] and self-training [36,98] dominate almost all kinds of 2D scene adaptation scenarios [57,58,12,47,88,61,14]. Methods based on adversarial training adopt domain discriminators [26,55] to implicitly search for domain-invariant features via distance measurements at different levels, *i.e.*, input-level [29,44,70,86,85], feature-level [41,82,18], and output-level [72,75,76]. However, such methods suffer from high computational costs and tend to be sensitive to hyperparameters and target domain changes [43,32]. Self-training, on the other hand, offers a lighter option by jointly learning from both source and target domain supervisions [79], where the latter can be generated via confidence thresholding [38,100,101]. More recent works even combine self-training with style transfer [11,34,77] and adversarial pre-training [17,45,50,97]. Evidence shows that these methods – albeit powerful in 2D – become less effective in 3D [32,52], which motivates us to design new methods w.r.t. the characteristics of the LiDAR data, such as the spatial consistency of the range-view representation.

UDA on LiDAR Point Clouds. Adaptations are more challenging in the 3D world as point clouds are sparse, unstructured, and have limited visual cues compared to images [71]. Alonso *et al.* [2] proposed to use shifting to align domain appearances. ePointDA [95] learns a dropout noise rendering from real-world data to match synthetic data. LiDARNet [33] employs two discriminators that jointly adapt for segmentation and boundary prediction. Complete&Label [87] targets on cross-sensor UDA where sparsity rather than city discrepancies serves as the major domain gap, which is beyond the scope of this work. xMUDA [32] and DsCML [52] employ self-training alongside multi-modality learning for cross-city adaptations. However, the assumption of having access to synchronized RGB and LiDAR data in both source and target domains is not always practical, which limits such methods. Also, they use point/voxel-based backbones which require a huge amount of memory and suffer from low inference speed. Our framework is built upon mature 2D CNNs and does not require data from multiple modalities thus maintaining both simplicity and efficiency for practitioners.

Domain Mixed Inputs. Mixing-based strategies [92,91,15] have been widely adopted in fully- [84,60] and semi- [48,6,74] supervised learning tasks, but very few touched UDA. SimROD [56] proposed to create 2x2 collages with two source images (labels) and two target images (pseudo-labels) for robust object detection. DACS [70] cuts source objects out and pastes them onto the target images, alongside mixing corresponding source labels and target pseudo-labels. While the former [56] can corrupt the semantic consistency, the latter [70] requires extra costs for the “copy-paste” operation and lacks mixing background and target objects. Our ConDA provides more fine-grained interactions in-between domains and the concatenations are performed on the fly during self-training (via simple `torch.cat` or `tf.concat`) with almost zero cost.

Regularization. Anti-aliasing filters are popularly applied to reduce the aliasing artifacts in networks [73,93,99]. Such regularizers, however, have not been used in UDA. We conjecture that this is because the empirical observations re-

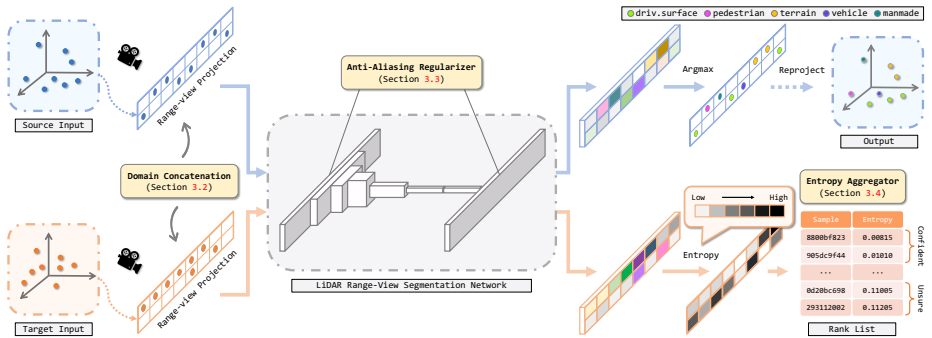


Fig. 2. Overview of our concatenation-based domain adaptation (ConDA) framework. After preprocessing (Sec. 3.1), sample stripes from the **source** domain and **target** domain are mixed via RV concatenation (Sec. 3.2). The concatenated inputs are fed into the segmentation network for feature extraction and prediction. We include anti-aliasing regularizers inside convolution operations (Sec. 3.3) to suppress the learning of high-frequency aliasing artifacts. The segmented RV cells are then projected back to the point clouds. Here the target prediction part is omitted for simplicity. To mitigate the impediment caused by erroneous target predictions, we design an entropy aggregator (Sec. 3.4) which splits target samples into a confident set and an unsure set and disables the usage of samples from the latter set.

quired in filter design become impractical on the annotation-void target domain. In this work, we adopt a learning-based approach as an alternative to regularize aliasing artifacts during network training. Another type of regularization is uncertainty estimation, which has been proved useful in semi-supervised learning [27]. For UDA, [78] proposed to resample more source data that contain high entropy classes in target predictions. IntraDA [50] uses a discriminator to close the gap between the low-entropy and high-entropy samples. We design an entropy aggregator to disable the usage of non-confident pseudo-labels during domain adaptation, which does not rely on extra discriminator network and directly reduces the uncertainty for the intermediate domain supervisions.

3 Technical Approach

The proposed ConDA consists of three major components as shown in Fig. 2. We first document the generic layout for LiDAR segmentation in range-view (RV) as preliminaries (Sec. 3.1). The domain concatenation strategy leverages the advantage of RV representations for constructing the intermediate domain (Sec. 3.2). To further improve the pre-training on the source domain and self-training on the intermediate domain, we design an anti-aliasing regularizer (Sec. 3.3) and an entropy aggregator (Sec. 3.4) to reduce the aliasing artifacts and noisy target predictions. The overall training procedure is summarized in Algo. 1.

3.1 Preliminaries

RV Projection. Let \mathcal{A} denote LiDAR point clouds. We project each point $\mathbf{o} = (x, y, z)$ on the 360° scans in \mathcal{A} via a mapping $\Pi : \mathbb{R}^3 \mapsto \mathbb{R}^2$ to a cylindrical RV image $\mathbf{a} \in \mathbb{R}^{(6,h,w)}$ with height h and width w [46]. To cover more points, h is set based on the number of rings for the LiDAR sensors, and w is determined by the horizontal angular resolution. Each pixel in \mathbf{a} is composed of the point coordinates (x, y, z) , intensity, range $\|\mathbf{o}\|_2$, and a binary mask (indicates whether or not a point occupies a pixel). The closest point to the sensor is chosen to represent the pixel if multiple points are projected to the same pixel location. Samples from the source domain $\mathcal{D} = s$ and target domain $\mathcal{D} = t$ are processed by the same operations. Note that the RV projection preserves the range information and the spatial correspondence for the LiDAR scans, *e.g.*, the near-front and far-front points are projected onto the left-bottom and left-top of the RV images, respectively, which is a unique feature of the LiDAR representations.

Segmentation Network. To extract features from \mathbf{a} efficiently, we design a fully-convolutional network \mathcal{G} with strided convolutions [39] and skip-connections [28] as our backbone. \mathcal{G} consists of seven stages (*cf.* Fig. 2). Since h is much smaller than w , we only downsample the height at later stages. The segmentation head combines the upsampled output features from the last four stages for multi-scale feature aggregations. Compared to previous RV networks [81,83,46,1,13,3], our backbone offers much better trade-off between accuracy and speed, which is essential for LiDAR UDA. More details on this aspect are placed in Appendix.

3.2 Domain Concatenation

In the context of UDA for LiDAR segmentation, we denote samples from the labeled source domain and unlabeled target domain as $\mathcal{A}_s = \{\mathbf{a}_s^i, \mathbf{y}_s^i\}_{i=1}^M$ and $\mathcal{A}_t = \{\mathbf{a}_t^j\}_{j=1}^N$, where M and N are the total number of source and target samples. For segmentation with C classes, the network \mathcal{G} can be optimized in a supervised way with source samples by minimizing the cross-entropy loss as follows:

$$\min_{\mathbf{w}} \mathcal{L}_s = -\frac{1}{|M|} \sum_{\mathbf{a}_s \in M} \sum_{c=1}^C \mathbf{y}_s^{(c)} \log p(c|\mathbf{a}_s, \mathbf{w}), \quad (1)$$

where \mathbf{w} denotes the weights of \mathcal{G} ; $p(\cdot)$ is the probability of class c in the softmax output. Due to the lack of ground-truth in the target domain, we consider the target labels as hidden variables [36] and select the most confident target predictions on the existing model as one-hot “pseudo-labels” $\hat{\mathbf{y}}_t$. The learning objective for the target domain is:

$$\begin{aligned} \min_{\mathbf{w}} \mathcal{L}_t &= -\frac{1}{|N|} \sum_{\mathbf{a}_t \in N} \sum_{c=1}^C \hat{\mathbf{y}}_t^{(c)} \log p(c|\mathbf{a}_t, \mathbf{w}), \\ \text{s.t. } \hat{\mathbf{y}}_t &= \begin{cases} \arg \max_c p(c|\mathbf{a}_t, \mathbf{w}), & \text{if } \max(p(c|\mathbf{a}_t, \mathbf{w})) \geq \theta \\ \text{ignored,} & \text{otherwise} \end{cases} \end{aligned} \quad (2)$$

where θ is a threshold for filtering non-confident pseudo-labels. Similar to [100,101], we set a proportion parameter k to determine the class-wise thresholds θ_c for each class c to balance the class distributions.

Now given a source batch $\{\mathbf{a}_s, \mathbf{y}_s\}$ and a target batch $\{\mathbf{a}_t, \hat{\mathbf{y}}_t\}$, our intermediate domain construction mechanism $\mathcal{M}(\cdot)$ follows three steps. First, define a template for the total number of segregation regions along the near-far dimension (m) in the RV projections and around the ego-vehicle (n). Fig. 1a shows an example of a domain concatenation with $m = 2$ and $n = 2$, having front-near, front-far, back-near, and back-far regions, respectively. Second, slice regions based on the above template for every sample in both batches. This gives $((b_s + b_t) \times m \times n)$ sliced stripes, where b_s and b_t are the batch sizes. Third, concatenate the stripes while keeping their spatial locations consistent, resulting in $(b_s + b_t)$ intermediate domain samples \mathbf{a}_π . Their labels \mathbf{y}_π can be obtained via the same arrangement of the original labels and pseudo-labels. The segmentation loss \mathcal{L}_π for this intermediate domain can be computed using the mixed batch $\{\mathbf{a}_\pi, \mathbf{y}_\pi\}$ in a way similar to Eq. 1. The overall objective for self-training is to minimize the following:

$$\mathcal{L} = \mathcal{L}_s(\mathbf{w}, \mathbf{y}_s) + \sigma \cdot \mathcal{L}_\pi(\mathbf{w}, \mathbf{y}_\pi), \quad (3)$$

where σ is a coefficient that controls the probability of accessing the intermediate domain. As shown in Fig. 1c, this simple concatenation approach mixes objects and background from both domains, while still preserving the overall consistency. This stability in semantic coherence comes from the priors that the LiDAR point clouds are unstructured and extremely sparse even after RV projections. Take the popularly adopted nuScenes [7] dataset as an example. We find that on average 59.93% of RV cells are empty, which could downplay the negative impact of region rearrangement since the degree of continuity is low. Besides, the spatially corresponding regions in RV tend to contain similar objects and background, regardless of the domain shift. A typical example is the ‘driveable surface’ class, which occupies more than 56% of cells in the bottom-half RV projections for both cities (correspond to two domains) in nuScenes [7]. We provide more concrete evidence in the Appendix to support our findings.

3.3 Anti-Aliasing Regularizer

Motivated by the recent findings that removing aliasing artifacts in the convolutional networks can improve generalizability [73], we formulate an anti-aliasing regularizer that is built within each convolution filter in the segmentation network to reduce learning from aliasing artifacts. Our goal is to impose regularization on high-frequency representation learning since they are more susceptible to aliasing artifacts [93,99]. We achieve this via $\mathbf{f}_{c,r} = \mathbf{f}_r \odot \mathbf{f}_c$, where \mathbf{f}_r denotes our regularizer which consists of learnable parameters having the same size as the convolution filter \mathbf{f}_c ; $\mathbf{f}_{c,r}$ is the regularized filter kernel of each convolution; \odot denotes the Hadamard multiplication. Note that during the earlier stages of training, the network tends to learn low-frequency representations [8,63] that

are robust to aliasing artifacts. This will thereby update \mathbf{f}_r such that it becomes more suited for low-frequency representation learning of $\mathbf{f}_{c,r}$. In later phases of training or UDA self-training, however, the network is more inclined to learn increasingly higher frequency representations [8,63] and thus becomes more susceptible to aliasing artifacts [73]. The modulation of our \mathbf{f}_r on \mathbf{f}_c regularizes gradient updates corresponding to these high-frequency representations and in particular, regularizes the ones that are considerably different from the earlier network learning. This implicit regularization mechanism at later stages of training makes $\mathbf{f}_{c,r}$ more resistant to high-frequency aliasing artifacts than the plain convolution filter \mathbf{f}_c . Note that, since \mathbf{f}_c and \mathbf{f}_r are both constants during inference, the regularized filter kernel $\mathbf{f}_{c,r}$ only needs to be computed once at the end of training and then can be used at inference without adding any additional computational cost or structural changes to the network – this makes our regularizer unique among all previous anti-aliasing mechanisms.

3.4 Entropy Aggregator

Given the fact that the pseudo-labels generated from the source pre-trained model tend to be noisy [78], we design an entropy aggregator to disable the access of non-confident target predictions and thus improve the overall quality of the intermediate domain supervisions. More formally, given a target sample \mathbf{a}_t , its entropy map \mathcal{E} composed of the normalized pixel-wise entropies can be calculated as follows:

$$\mathcal{E} = \frac{-1}{\log(C)} \sum_{c=1}^C p(c|\mathbf{a}_t, \mathbf{w}) \log p(c|\mathbf{a}_t, \mathbf{w}). \quad (4)$$

The median value \mathbf{e} of \mathcal{E} for each \mathbf{a}_t is used as the global-level indicator of uncertainty, which is more robust than the average value due to the large “noisy” predictions for the empty RV cells. The target set $\mathcal{A}_t = \{\mathbf{a}_t^j\}_{j=1}^N$ is re-organized based on \mathbf{e} and only the pseudo-labels from the top ϖ most confident target samples are included as the supervisions for the intermediate domain (*cf.* Sec. 3.2).

Integrating our technical contributions, we now present the overall training procedure of ConDA (*cf.* Algo. 1), which consists of two rounds of self-training that encourage fine-grained interactive learning in-between domains while regularizing anti-aliasing artifacts and non-confident target predictions. As we will show in the next section, these components are complementary to each other and the marriage of them can significantly boost the adaptation performance.

4 Experiments and Analysis

4.1 Settings

Data. We construct two RV-based cross-city UDA scenarios with nuScenes [7] – a large-scale autonomous driving database widely adopted in academia. It consists of 1000 driving scenes with 40k annotated keyframes taken at 2Hz.

Algorithm 1 ConDA Self-Training Procedure

- 1: **Input:** Source data and labels $\{\mathbf{a}_s, \mathbf{y}_s\}$; target data $\{\mathbf{a}_t\}$; pre-trained weights \mathbf{w}^{r0} ;
Param: Entropy threshold ϖ , proportion threshold k , concatenation probability σ
 - 2: **Output:** Self-trained backbone weights \mathbf{w}^{r2}
 - 3: **Round 1:**
 - 4: Calculate median entropy $\mathbf{e} = \text{mid}(\mathcal{E})$ for all \mathbf{a}_t with \mathbf{w}^{r0} via Eq. (4)
 - 5: Sort $\{\mathbf{a}_t\}$ in an ascending order based on \mathbf{e}
 - 6: Keep the top ϖ most confident $\{\mathbf{a}_t\}$ and discard the rest $\rightarrow \{\mathbf{a}_t\}_\varpi$
 - 7: Generate pseudo-labels $\{\hat{\mathbf{y}}_t\}_\varpi$ with k , \mathbf{w}^{r0} via Eq. (2)
 - 8: **repeat**
 - 9: $\{\mathbf{a}_\pi^{r1}, \mathbf{y}_\pi^{r1}\} = \mathcal{M}(\{\mathbf{a}_s, \mathbf{y}_s\}, \{\mathbf{a}_t, \hat{\mathbf{y}}_t\}_\varpi)$ (*cf.* Sec. 3.2)
 - 10: Calculate loss $\mathcal{L}(\mathcal{L}_s, \mathcal{L}_\pi)$ with σ via Eq. (3); update weights
 - 11: **until** convergence $\rightarrow \mathbf{w}^{r1}$
 - 12: **Round 2:**
 - 13: Generate pseudo-labels $\{\hat{\mathbf{y}}_t\}$ with k , \mathbf{w}^{r1} via Eq. (2)
 - 14: **repeat**
 - 15: $\{\mathbf{a}_\pi^{r2}, \mathbf{y}_\pi^{r2}\} = \mathcal{M}(\{\mathbf{a}_s, \mathbf{y}_s\}, \{\mathbf{a}_t, \hat{\mathbf{y}}_t\})$ (*cf.* Sec. 3.2)
 - 16: Calculate loss $\mathcal{L}(\mathcal{L}_s, \mathcal{L}_\pi)$ with σ via Eq. (3); update weights
 - 17: **until** convergence $\rightarrow \mathbf{w}^{r2}$
-

We split samples based on their geographic locations. This gives 15695 and 12435 training samples and 3090 and 2929 evaluation samples for Boston and Singapore, respectively. All training samples are used as the source/target for adaptations. Different from xMUDA [32] which only assigns semantic labels to points inside bounding boxes with 4 object classes and 1 background class, we adopt the *lidarseg*⁵ subset in nuScenes which contains 16 classes and fine-grained point-level annotations for LiDAR segmentation.

Implementation Details. The point clouds are transformed into RV images of size 32×1920 as the inputs for the segmentation network (*cf.* Sec. 3.1). It is first trained from scratch with only source samples for 80 epochs with a batch size of 24 and then fine-tuned under our entropy aggregator-guided self-training procedure (*cf.* Algo. 1). Both rounds are trained for 20 epochs with the same batch size. We denote results for the supervised learning and direct adaptation as “oracle” and “source-only”. Since this is a new benchmark, we could only compare ConDA with state-of-the-art adversarial [72,75,76], self-training [100,38,50], and consistency training [67,10] methods originally tested for 2D adaptations. We replace their backbones with our RV network and keep other configurations in default. The AdamW [40] optimizer is adopted ($\beta_1 = 0.9$, $\beta_2 = 0.999$) with the OneCycle [64] scheduler for pre-training (with learning rate 1e-3) and the Step scheduler for self-training (with learning rate 1e-4). For data augmentation, we first employ yaw rotation, jitter, axis flipping, and scaling to the original point clouds and then project augmented points onto RV. For methods based on self-training, we generate their pseudo-labels offline as in [38,100]. All methods are implemented using PyTorch on NVIDIA Tesla V100 with 16GB RAM.

⁵ More details at: <https://www.nuscenes.org/nuscenes#lidarseg>.

Table 1. Effectiveness for each component in ConDA. **AA**: anti-aliasing regularizer; **DC**: domain concatenation; **EA**: entropy aggregator. **MR**: multi-round self-training. All IoU scores are given in percentage (%).

AA DC EA MR	barr	bicy	bus	car	const	moto	ped	cone	trail	truck	driv	othe	walk	terr	mann	veg	FIoU	mIoU
Source-only	29.3	1.3	52.0	71.4	7.2	11.7	42.6	12.2	0.0	30.4	85.9	12.7	32.6	41.0	62.5	65.9	64.3	34.9
Baseline	39.4	5.3	66.1	75.6	9.3	20.7	47.8	14.9	0.0	34.1	88.4	25.5	38.1	49.9	66.7	68.5	68.6	40.7
✓	42.6	4.6	67.5	73.2	10.1	23.1	51.4	14.0	0.0	39.3	88.1	24.9	38.1	56.0	66.8	70.5	70.0	41.9
✓ ✓	44.6	4.1	68.1	75.1	11.9	29.6	53.5	15.7	0.0	39.6	88.5	32.1	38.2	59.6	67.9	73.9	71.2	43.9
✓ ✓ ✓	52.6	6.4	70.2	77.2	11.9	25.6	51.8	15.2	0.0	43.4	90.7	38.6	42.1	57.5	68.6	72.6	72.4	45.3
✓ ✓ ✓ ✓	51.4	5.0	70.6	77.0	12.6	30.8	52.5	16.7	0.0	41.3	90.5	38.8	43.9	59.7	69.8	73.8	73.3	45.9
✓ ✓ ✓ ✓ ✓	54.1	6.8	67.4	77.2	12.1	38.7	51.8	16.0	0.0	44.0	90.4	38.7	44.0	62.9	70.7	75.0	74.1	46.9

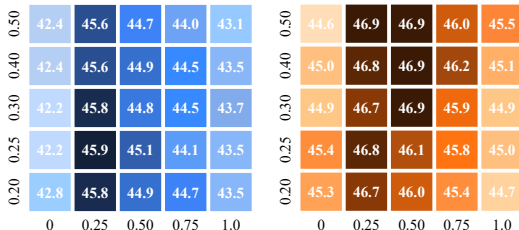
Evaluation Metrics. We follow the conventional reporting of the intersection-over-union (IoU) scores (%) over each class, the mean IoU (mIoU) and the frequency-weighted IoU (FIoU) scores (%) over all classes in our experiments.

4.2 Ablation Studies

Q1: What is the effect for each component in ConDA?

A1: We adopt the Boston \rightarrow Singapore setting in our ablation studies without the loss of generality. We stratify the three major components in our framework and show their impacts in Tab. 1. Specifically, the anti-aliasing regularizer offers an improvement of 1.2% mIoU over the baseline and surpasses the source-only case by 7.0% mIoU. Comparing the frequency spectrum of 3x3 kernels from the network, we also find that the ratio of ‘average low-frequency amplitudes’ to ‘average high-frequency amplitudes’ is 23.2% higher (statistically significant with t-test: $p < 0.001$) for the network trained with our regularizer. On top of that, our domain concatenation further improves 3.4% mIoU. Another boost of 1.6% mIoU is achieved under the two-round guidance self-training of our entropy aggregator. Overall, our framework significantly improves the adaptation results from 34.9% mIoU to 46.9% mIoU, which corresponds to nearly a 34.4% relative improvement over the source-only and 6.2% mIoU higher than the baseline. We provide additional ablation examples and visualizations in Appendix.

Fig. 3. Sensitivity analysis for the concatenation probability σ (horizontal axis) and proportion threshold k (vertical axis) in self-training round 1 (left) and round 2 (right). Numbers reported are mIoU scores in percentage (%). The darker the color, the higher the score.



Q2: What are the optimal hyperparameters for ConDA?

A2: We conduct extensive experiments to show the best possible selections for the hyperparameters in our framework. Specifically, the vertical and horizontal

Table 2. Sensitivity analysis for entropy threshold ϖ .

ϖ	0.0625	0.1250	0.1875	0.2500	0.3125	0.3750	0.4375	0.5000	0.5625	0.6250	0.6875	0.7500	0.8125	0.8750	0.9375	1.000
mIoU	43.1	45.0	45.0	45.3	45.4	45.7	45.7	45.9	45.9	45.8	45.7	45.8	45.5	45.4	45.2	45.3

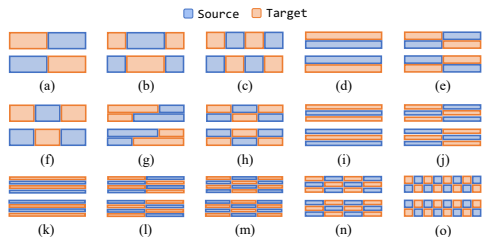
Table 3. Adaptation results for different RV concatenation strategies (*cf.* Fig. 4) and other mixing techniques. Numbers reported are mIoU scores in percentage (%).

Method	w/o	a	b	c	d	e	f	g	h	i	j	k	l	m	n	o	[56]	[92]	[15]	[91]
mIoU	41.9	43.4	43.5	43.7	44.5	44.6	43.9	44.5	44.6	45.3	45.0	45.2	45.3	44.9	44.6	44.2	33.7	41.1	43.1	42.6

axes of Fig. 3 show the impact for the proportion parameter k and the concatenation parameter σ during the two-round self-training while Tab. 2 gives the sensitivity results for the entropy regularization parameter ϖ . We find that lower values for k (*e.g.* 0.25) in round 1 and relatively higher values (*e.g.* 0.5) in round 2 tend to give higher mIoU. We conjecture that this relatively conservative choice (or lower value) at round 1 is helpful since pseudo-labels tend to be noisy at this stage. The quality of pseudo-label gets much better in round 2 and including more of them gives a positive impact on the performance. As for σ , we observe that the best possible scores are achieved in between 0.25 and 0.50. Training without ($\sigma = 0$) or with all ($\sigma = 1$) concatenated samples does not perform well. For ϖ (after setting both k and σ as 0.25 without the loss of generality), we find that large ϖ involves more false positives while small ϖ limits the diversity. A compromise value like 0.50 gives the best possible scores.

Q3: What is the best practice for RV concatenation?

A3: Besides the intuitive front-back RV concatenation, we also consider other scenarios as in Fig. 4 and show their results in Tab. 3. As shown, strategies i and l perform the best while j and k offer competitive results. We note that: 1) increasing the granularity of the interactions between source and target tends to improve performance (strategies a to l); 2) increasing the granularity beyond a certain limit (strategies m , n , and o) can deteriorate performance, which is likely due to the instability in semantic coherence of the objects and background in the concatenated stripes;

**Fig. 4.** Various RV concatenation strategies.

and 3) fine-grained interactions along the vertical axes, *i.e.*, near to far regions, perform better than interactions along the horizontal axes, *i.e.*, bearing around the ego-vehicle (strategies i and f), suggesting that the former likely yields better domain interactions while better maintaining the semantic consistency.

Q4: How is domain concatenation superior to others?

A4: We compare our domain concatenation with four mixing techniques in Tab. 3. SimROD [56] stitched samples from both domains as inputs for adaptation while MixUp [92], CutMix [91], and CutOut [15] are general regularization

Table 4. Adaptation results for **Boston** \rightarrow **Singapore**. The methods are grouped, from top to bottom, as adversarial training, self-training, both, and ours. All IoU scores are given in percentage (%). Best score for each class is highlighted in **bold**.

Method	barr	bicy	bus	car	const	moto	ped	cone	trail	truck	driv	othe	walk	terr	manm	veg	FloU	mIoU
Oracle	79.5	33.6	87.5	88.9	37.6	75.6	70.5	50.3	0.0	76.2	95.1	53.7	60.2	74.4	83.4	85.5	84.2	65.8
Source-only	29.3	1.3	52.0	71.4	7.2	11.7	42.6	12.2	0.0	30.4	85.9	12.7	32.6	41.0	62.5	65.9	64.3	34.9
AdaptSeg [72]	28.0	7.2	60.9	70.7	7.7	17.4	45.5	14.3	0.0	36.4	88.1	28.4	36.0	43.1	63.0	66.7	66.1	38.3
MinEnt [75]	31.7	4.0	63.7	70.6	5.8	15.9	47.7	13.7	0.1	34.9	87.9	22.4	37.5	41.5	59.9	62.2	64.3	37.5
AdvEnt [75]	28.7	5.9	59.4	76.4	7.2	18.2	50.6	16.7	0.0	32.6	87.0	28.1	36.6	44.0	63.9	67.1	66.3	38.9
DADA [76]	27.4	4.9	60.0	67.7	7.3	15.9	44.4	14.7	0.0	33.9	87.1	21.2	34.9	42.1	62.2	64.9	64.8	36.8
BDL _{PL} [38]	39.2	0.3	53.0	73.2	6.8	16.0	40.2	8.5	0.0	29.8	88.7	21.3	39.7	48.5	67.1	67.9	68.3	37.5
CBST [100]	39.4	5.3	66.1	75.6	9.3	20.7	47.8	14.9	0.0	34.1	88.4	25.5	38.1	49.9	66.7	68.5	68.6	40.7
AdaptSeg _{PL} [72]	29.9	0.3	47.9	64.4	4.9	7.4	28.4	4.6	0.0	24.8	83.1	21.8	38.3	46.5	67.1	68.9	66.0	33.7
IntraDA [50]	28.0	5.6	57.8	76.1	6.2	18.6	47.4	13.8	0.0	32.1	87.3	27.6	37.0	44.4	63.4	66.5	66.2	38.3
ConDA (Ours)	54.1	6.8	67.4	77.2	12.1	38.7	51.8	16.0	0.0	44.0	90.4	38.7	44.0	62.9	70.7	75.0	74.1	46.9

Table 5. Adaptation results for **Singapore** \rightarrow **Boston**. The methods are grouped, from top to bottom, as adversarial training, self-training, both, and ours. All IoU scores are given in percentage (%). Best score for each class is highlighted in **bold**.

Method	barr	bicy	bus	car	const	moto	ped	cone	trail	truck	driv	othe	walk	terr	manm	veg	FloU	mIoU
Oracle	71.3	35.5	71.5	86.9	41.6	35.4	69.7	61.2	57.6	68.0	95.9	70.7	79.7	58.7	89.9	83.9	88.5	67.3
Source-only	15.5	7.9	20.6	70.5	16.1	3.6	41.9	11.4	0.5	40.6	90.2	10.7	41.7	19.1	77.4	74.5	73.4	33.9
AdaptSeg [72]	15.9	2.4	40.4	73.9	15.2	5.5	48.3	8.3	0.4	46.3	92.2	18.7	54.5	19.0	79.0	70.9	76.2	36.9
MinEnt [75]	19.2	0.2	36.1	73.2	15.7	6.2	50.3	10.8	0.8	45.0	91.5	24.1	54.8	21.7	78.7	71.8	76.0	37.5
AdvEnt [75]	12.5	9.0	43.0	74.1	14.7	7.0	51.4	12.7	0.5	47.0	91.4	14.5	53.6	19.2	80.1	73.4	76.2	37.8
DADA [76]	18.5	2.9	35.5	73.0	15.0	6.5	49.3	11.0	1.6	43.6	91.8	12.2	52.7	19.7	79.8	73.4	76.1	36.7
BDL _{PL} [38]	18.9	2.7	30.8	75.8	13.3	3.8	45.4	7.4	1.8	45.4	92.8	19.7	58.4	18.7	80.1	76.3	77.6	37.0
CBST [100]	17.7	1.4	33.6	75.0	13.3	6.4	52.3	12.3	1.9	46.9	92.5	22.8	57.2	19.7	80.2	77.3	77.5	38.1
AdaptSeg _{PL} [72]	10.5	0.6	33.5	71.3	17.2	5.2	41.9	11.4	1.0	43.5	90.4	18.5	60.1	20.0	80.0	74.6	76.1	36.3
IntraDA [50]	12.3	6.2	41.2	73.4	14.1	5.6	43.5	13.4	0.7	48.1	91.2	16.4	54.1	18.8	79.2	70.6	75.7	36.8
ConDA (Ours)	11.8	9.0	49.1	76.3	7.2	18.0	62.6	15.2	0.0	47.9	92.3	34.9	59.4	27.9	83.2	82.3	79.3	42.3

methods adopted for fully- and semi-supervised learning. While all four methods achieve promising results in their respective RGB-based tasks, they have shown sub-par performance in the RV representation for UDA in LiDAR segmentation. Differently, our approach is able to effectively leverage the spatial context of RV, and combine both the source and target domains into an intermediate domain for fine-grained interactive learning and regularization.

4.3 Comparison to State-of-the-Art

Benchmarking Results. We compare ConDA with eight state-of-the-art methods on the Boston \rightarrow Singapore and Singapore \rightarrow Boston scenarios in Tab. 4 and Tab. 5. In both cases, ConDA substantially outperforms other competitors in terms of mIoU and FloU. We observe relatively higher adaptation scores for static classes such as ‘driveable surface’ and ‘vegetation’ and lower scores for dynamic classes such as ‘barrier’ and ‘motor’. Notably, in contrast to prior approaches that tend to improve performance on relatively easier classes (*i.e.*,

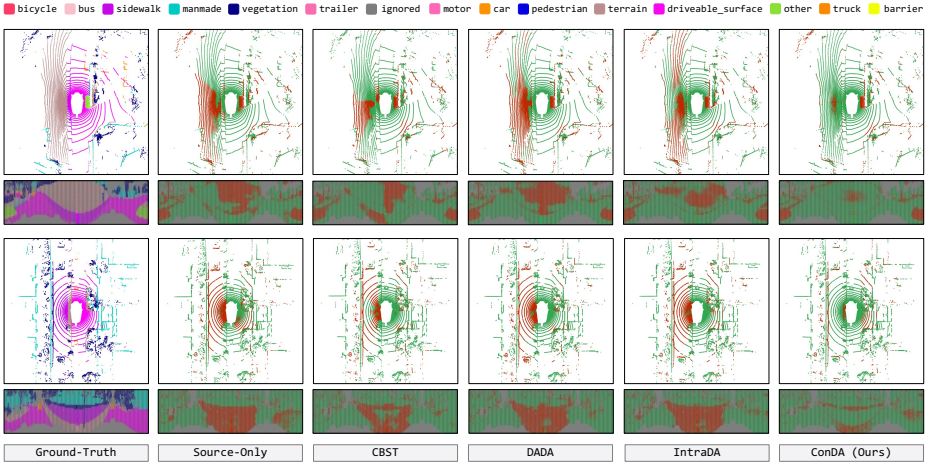


Fig. 5. Qualitative results from both the bird’s eye view and range-view. To highlight the difference between the predictions and ground-truth, the **correct** and **incorrect** points/pixels are painted in **green** and **red**, respectively. Best viewed in color.

classes on which the source-only has already performed well), ConDA yields considerable performance gains on almost all classes. This strongly supports our findings that fine-grained objects/background interactions in-between domains are conducive for closing the domain gap and thus improving the adaptations.

Qualitative Assessment. Fig. 5 presents several visualization results for different methods, *i.e.*, self-training (CBST [100]), adversarial training (DADA [76]), and both (IntraDA [50]). We observe that while the prior arts can only give limited improvements in certain areas, ConDA mitigates the false predictions holistically in most regions around the ego-vehicle. We accredit this to both the generalization ability provided by domain concatenation and the regularization enhancement offered by our anti-aliasing regularizer and entropy aggregator.

Training Complexity. Fig. 6 shows the training time of different methods. Note that the pseudo-label generation time⁶ is excluded since this operation is conventionally conducted offline [32,100,38]. We find that



Fig. 6. Training time (in hours) for each method.

while the inference speeds for these methods are similar (since they are sharing the same range-view segmentation backbone), ConDA is still faster than most adversarial methods [72,75,76] which rely on additional discriminators for learning domain-invariant features during the adaptation. Our work is comparable

⁶ Around 1 hour for the Boston → Singapore and Singapore → Boston scenarios with nuScenes [7]; might vary among different databases.

Table 6. SSDA results. Left-half: results for **Boston** \rightarrow **Singapore**; Right-half: results for **Singapore** \rightarrow **Boston**. Numbers are mIoU scores in percentage (%).

Method	Source	+0.1%	+1%	+10%	+20%	+50%	Oracle	Source	+0.1%	+1%	+10%	+20%	+50%	Oracle
MeanTeacher [67]		7.8	17.1	25.7	28.4	37.7			22.1	24.4	47.6	49.3	61.2	
CPS [10]		17.1	29.5	38.2	45.8	54.8			30.3	32.0	41.5	56.1	62.8	
AdaptSeg [72]		40.3	45.0	55.0	58.6	63.1			40.0	45.9	58.2	62.1	66.9	
MinEnt [75]	34.9	39.8	45.3	54.9	59.3	63.3	65.8	33.9	39.6	47.0	58.9	61.8	66.7	67.3
AdvEnt [75]		41.7	46.0	55.4	59.4	62.5			39.6	46.5	59.9	62.2	66.7	
DADA [76]		40.2	45.3	54.2	59.0	62.2			39.5	45.8	59.2	62.5	67.5	
CBST [100]		45.2	51.5	59.3	61.7	64.4			40.9	49.7	60.7	63.2	67.0	
ConDA (Ous)		48.1	53.8	62.6	65.3	67.4			42.5	51.6	62.6	65.5	70.0	

Table 7. WSDA results. Left-half: results for **Boston** \rightarrow **Singapore**; Right-half: results for **Singapore** \rightarrow **Boston**. Numbers are mIoU scores in percentage (%).

Method	Source	+0.1%	+1%	+10%	+20%	+50%	Oracle	Source	+0.1%	+1%	+10%	+20%	+50%	Oracle
Labeled-only		52.6	59.6	62.8	62.6	63.0			50.5	59.8	63.6	64.1	64.8	
MeanTeacher [67]		53.3	59.2	62.6	64.0	64.5			52.3	62.5	65.2	65.8	65.9	
CPS [10]		55.1	59.5	64.2	64.9	64.1			50.8	62.9	66.1	66.4	67.0	
AdaptSeg [72]	34.9	53.1	59.6	61.5	62.4	62.8	65.8	33.9	51.7	59.9	61.9	63.9	64.8	67.3
MinEnt [75]		53.5	59.8	61.8	62.1	62.7			50.7	60.0	63.8	64.6	64.9	
AdvEnt [75]		53.3	58.9	62.6	62.8	62.4			52.9	59.6	63.3	63.9	61.8	
DADA [76]		53.6	58.5	62.3	62.5	63.5			51.7	60.5	62.3	63.5	63.6	
ConDA (Ous)		55.9	61.4	65.9	67.2	67.3			52.9	64.8	68.6	70.8	71.4	

with MinEnt [75] and CBST [100] in terms of speed but provides much better adaptation performance.

4.4 Practical Extension

In practice, annotating a small set of target data (semi-supervised domain adaptation, SSDA) or a small part of points for each target point cloud (weakly-supervised domain adaptation, WSDA) is acceptable. To this end, we relax the UDA constraint by involving certain proportions of target annotations and treating the remaining ones as unlabeled. We establish these two adaptation settings by involving 0.1%, 1%, 10%, 20%, 50% uniformly selected target samples/points and show their results in Tab. 6 and Tab. 7. It can be seen that the domain gap can be overtly mitigated by involving a small set (*e.g.* 1%) of labeled target data. It is worth noting that for SSDA/WSDA with only 20%/10% target annotations, ConDA is able to approach the oracle performance and even surpasses it if a 50%/20% quota is allowed. The results verify again that ConDA brings strong augmentation and regularization capabilities during adaptations.

5 Conclusion

We presented ConDA, a concatenation-based domain adaptation framework that leverages the spatial coherency in-between the source and target domains for fine-grained interactive learning. We also introduced an anti-aliasing regularizer and an entropy aggregator to reduce the detrimental effects of aliasing artifacts

and noisy target predictions during pre-training and self-training. Extensive experiments on cross-city UDA/SSDA/WSDA scenarios showed that ConDA can substantially improve the segmentation performance over baseline and competitive approaches. The robustness of our framework has shed light on its utility and potential for flexible deployment in perception modules of the autonomous driving system. In the future, we intend to dive deeper into the interactions in-between domains and to extend our framework to other LiDAR domain adaptation scenarios, such as night/day, sunny/rainy, and synthetic/real adaptations.

Appendix

This appendix is organized as follows:

- Section 6 presents the statistics and visualizations for the domain discrepancies in our cross-city domain adaptation scenarios (*cf.* Sec. 3.2).
- Section 7 contains the detailed procedure for LiDAR range-view projection (*cf.* Sec. 3.1), more details for our segmentation network (*cf.* Sec. 3.1), and discussions for our anti-aliasing regularizer (*cf.* Sec. 3.3).
- Section 8 provides the detailed/complete quantitative and qualitative results for our ablation studies (*cf.* Sec. 4.2) and comparative studies (*cf.* Sec. 4.3).
- Section 9 elaborates more details on the practical extensions of the semi-supervised domain adaptation (SSDA) and weakly-supervised domain adaptation (WSDA) settings (*cf.* Sec. 4.4).

6 Domain Discrepancy

6.1 Statistics

Sparsity. Different from the densely populated RGB representations such as images and videos, the LiDAR point clouds are naturally sparse. As a concrete example, we calculate the total number of valid (w/ semantic labels) and empty (w/o semantic labels or w/ ignored labels) range-view cells for the two splits in nuScenes⁷ [7]. We observe that only 37.59% (Boston) and 42.55% (Singapore) of cells contain semantic labels while on average 59.93% of cells are empty. Such a sparsity could downplay the negative impact of region rearrangements since the degree of continuity for this type of representation is low. Note that the position encoding (*e.g.* the point coordinates (x, y, z) and range $\|\mathbf{o}\|_2$) plays an important role in the feature representations of LiDAR point clouds. Our domain concatenation strategy maintains the integrity of such encoding by keeping the spatial locations of the rearranged stripes consistent.

Inter-Discrepancy. The idiosyncrasies of cities and their geographic mismatches cause performance degradation during cross-city evaluations (*cf.* Tab. 4 and Tab. 5), *i.e.*, 65.8% \rightarrow 34.9% and 67.3% \rightarrow 33.9% mIoU drops for the Boston

⁷ Refer to the *lidarseg* set of the nuScenes [7] database in this work. More details at: <https://www.nuscenes.org/nuscenes#lidarseg>.

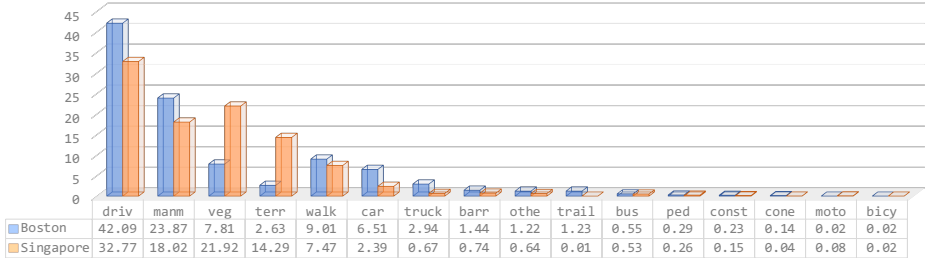


Fig. 7. A case study for cross-city domain discrepancies with nuScenes [7]. **Longitudinal comparison:** Samples from different locations (Boston and Singapore) follow different distributions (inter-discrepancy). **Horizontal comparison:** The proportions of different classes in the same location are severely imbalanced (intra-discrepancy). Table shows the percentage (%) that each semantic class occupies in the LiDAR range-view projection.

→ Singapore and Singapore → Boston adaptation scenarios, respectively. To further unveil the potential causes of such degradation, we calculate the class occupancy (in range-view) of the two cities in nuScenes [7] and show their distributions in Fig. 7. Specifically, we find that the Boston split contains more ‘barrier’ (1.9×), ‘car’ (2.7×), ‘traffic cone’ (3.5×), ‘trailer’ (123×), and ‘truck’ (4.4×), while the Singapore split has more ‘motor’ (4.0×), ‘terrain’ (5.4×), and ‘vegetation’ (2.8×). In hindsight, we conjecture that such class-wise discrepancies between domains lead to biased models trained towards the source domain, which brings difficulties when making predictions for the unseen target domain. Our proposed approach mitigates such discrepancies by mixing the domain distributions. The intermediate domain contains idiosyncrasies of both the source domain and target domain and training with samples from this mixed domain may enable the model to be more robust during cross-city domain adaptations.

Intra-Discrepancy. We also notice from Fig. 7 that the proportions of different classes in the same city are severely imbalanced. Large amounts of cells are occupied by the static classes, such as ‘driveable surface’, ‘manmade’, ‘vegetation’, and ‘terrain’, while those dynamic classes like ‘bicycle’ and ‘motor’ rarely occur. Such discrepancies inside domains may lead to biased models which favor the “dominant” classes while ignoring those “rare” classes. The class-wise IoU scores (cf. Tab. 4 and Tab. 5) also reflects such discrepancies, e.g., the source-only IoU scores for the ‘driveable surface’ class only drop 9.2% and 5.7% for the Boston → Singapore and Singapore → Boston adaptation scenarios, respectively, while the scores for the ‘barrier’ class degrade from 79.5% to 29.3% and 71.3% to 15.5%. Methods based on self-training have more chances to introduce the “rare” classes during model re-training/fine-tuning and thus resulting in better performance. Our approach follows and extends on this aspect by exchanging objects/background in-between domains and achieving better adaptation results.

Spatial Consistency. Although there are overt discrepancies between domains, we observe relatively stable distributions at certain regions in range-view. As shown in Tab. 8, the ratios between the top-half and the bottom-half stripes

Table 8. Class-wise occupancy in percentage (%) for the top-half and bottom-half LiDAR range-view splits in Boston (BS) and Singapore (SG).

Split	barr	bicy	bus	car	const	moto	ped	cone	trail	truck	driv	othe	walk	terr	mann	veg
Top-half (BS)	1.11	0.02	0.83	6.44	0.41	0.02	0.51	0.14	2.21	4.17	13.73	0.55	5.70	2.36	46.32	15.48
Bottom-half (BS)	1.75	0.01	0.29	6.56	0.07	0.02	0.08	0.16	0.34	1.81	68.05	1.84	12.03	2.88	3.32	0.78
Ratio (Top/Bottom)	0.63	2.00	2.86	0.98	5.86	1.00	6.38	0.88	6.50	2.30	0.20	0.30	0.47	0.82	13.95	19.85
Top-half (SG)	0.57	0.02	0.74	2.28	0.24	0.06	0.38	0.02	0.01	0.91	10.59	0.22	3.97	11.36	30.86	37.78
Bottom-half (SG)	0.09	0.01	0.30	2.53	0.04	0.11	0.13	0.05	0.06	0.41	56.94	1.10	11.29	17.48	4.02	4.65
Ratio (Top/Bottom)	6.33	2.00	2.47	0.90	6.00	0.55	2.92	0.40	0.17	2.22	0.19	0.20	0.35	0.65	7.68	8.12
Overall ratio (BS/SG)	1.94	1.00	1.04	2.72	1.53	0.25	1.12	3.50	123	4.39	1.28	1.91	1.21	0.18	1.32	0.36

for each domain are more consistent than the ratios between domains. This is mainly due to the common layouts of street scenes and the transformation consistency of range-view projection. Typical evidence of this is the distributions of the ‘driveable surface’ class and the ‘manmade’ class. While the former dominates the bottom-half plane in range-view (68.05% for Boston and 56.94% for Singapore), the latter is more likely to appear in the top-half regions (46.32% for Boston and 30.86% for Singapore). Such unique spatial layouts ensure the integrity of stripe rearrangements in-between domains since our approach avoids concatenating non-corresponding regions.

6.2 Visualization on Spatial Distribution

Dynamic Classes. We provide visual comparisons to illustrate the discrepancies between domains. As shown in Fig. 8, although different classes often behave distinctly in street scenes, the overall distributions for the dynamic classes (*e.g.*, ‘barrier’, ‘bus’, ‘car’, ‘truck’, ‘pedestrian’, etc.) are relatively consistent between domains. For example, the “vehicle” classes like ‘bus’, ‘car’, and ‘truck’ tend to appear in the middle of the left-half and right-half planes in the range-view projections, which correspond to the front-view and back-view of the ego-vehicle. Note that these dynamic classes have relatively low populations compared to the static ones due to the small object sizes and they tend to appear at certain regions in the street scenes. Encouraging the interactions of these classes in-between domains via domain concatenation has been proven conducive for the adaptations (*cf.* Tab. 4 and Tab. 5).

Statistic Classes. Due to the diverse idiosyncrasies of these two cities, the spatial layouts for the static classes, *i.e.*, ‘driveable surface’, ‘sidewalk’, ‘terrain’, ‘manmade’, and ‘vegetation’, tend to be different. For example, as shown in Fig. 8, the ‘driveable surface’ in Boston is wider than that in Singapore, while the ‘manmade’ and ‘vegetation’ in Singapore occupy more regions than that in Boston. As these idiosyncrasies cause biased models during training, it is thus beneficial to exchange the distributions (domain-specific information) of these classes so that the network is able to learn more robust and adaptable features from the concatenated intermediate domain. Moreover, in the case that mixing LiDAR range-view inputs is not likely to destroy semantic coherency (as

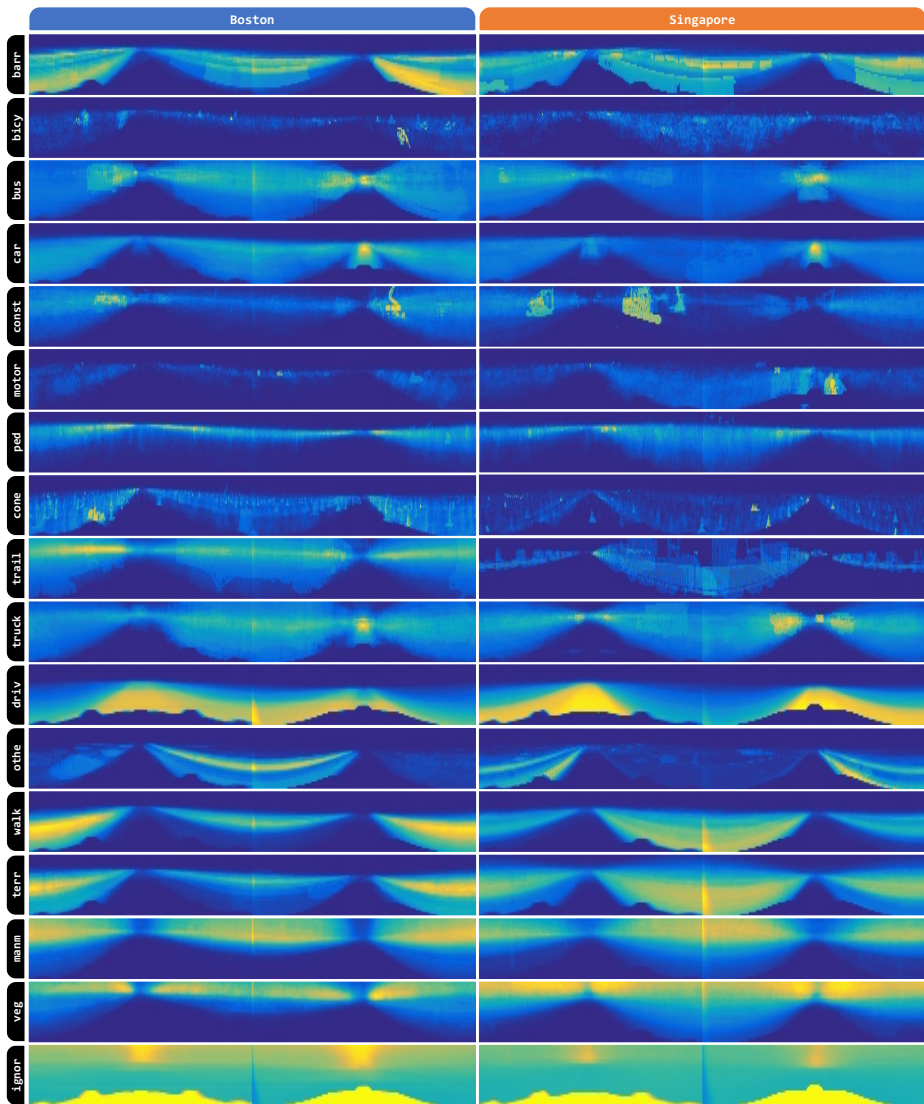


Fig. 8. Spatial priors in range-view (calculated via ground-truth) of each class for the Boston split and Singapore split in nuScenes [7]. Regions with lighter colors correspond to high-frequent occurrences and vice versa. Best viewed in color.

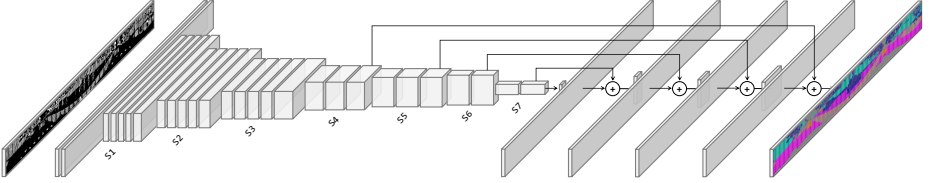


Fig. 9. The overall architecture of our segmentation network \mathcal{G} (cf. Sec. 3.1).

discussed in detail in Sec. 6.1), bridging domains can help to reduce the domain gap and thus improve adaptation performance.

7 Implementation Detail

7.1 Range-View Input

Cylindrical Projection. Given a LiDAR point cloud \mathcal{A} , we convert each point $\mathbf{o} = (x, y, z)$ inside \mathcal{A} to a structured cylindrical projection \mathbf{a} via a mapping $\Pi : \mathbb{R}^3 \mapsto \mathbb{R}^2$ as follows:

$$\begin{pmatrix} u \\ v \end{pmatrix} = \begin{pmatrix} \frac{1}{2} [1 - \arctan(y, x)\pi^{-1}] w \\ [1 - (\arcsin(z, r^{-1}) + \xi_{\text{up}})\xi^{-1}] h \end{pmatrix}, \quad (5)$$

where (u, v) denotes the cell coordinates of \mathbf{a} ; h and w are the height and width of \mathbf{a} set based on the number of sensor rings and the sensor horizontal angular resolution, respectively; $r = \|\mathbf{o}\|_2 = \sqrt{x^2 + y^2 + z^2}$ is the range between the point and the sensor; $\xi = |\xi_{\text{up}}| + |\xi_{\text{down}}|$ denotes the field-of-view (FOV) of the sensor where ξ_{up} is the vertical FOV at the upward direction and ξ_{down} is the horizontal FOV at the downward direction. In this work, we have $h = 32$, $w = 1920$, $\xi_{\text{up}} = 10.0$, and $\xi_{\text{down}} = -10.0$.

Feature Representations. For each pixel location (u, v) , we embed its point coordinate (x, y, z) , intensity (collected by the LiDAR sensor), range $\|\mathbf{o}\|_2$, and a binary mask (indicates whether or not a point occupies a pixel). This gives range-view pseudo-images $\mathbf{a} \in \mathbb{R}^{(6, h, w)}$ with six feature channels in total. LiDAR point clouds from both the source domain and the target domain are processed with the same operations, resulting in $\mathbf{a}_s \in \mathbb{R}^{(6, h, w)}$ and $\mathbf{a}_t \in \mathbb{R}^{(6, h, w)}$ source/target inputs, respectively.

7.2 Segmentation Network

Architecture. The overall architecture of our segmentation network \mathcal{G} (cf. Sec. 3.1) is shown in Fig. 9. Specifically, \mathcal{G} adopts the encoder-decoder hour-glass structure for feature extraction and prediction. It is composed of seven stages (S1 to S7), where each stage consists of several blocks for extraction, downsampling, upsampling, aggregation, etc. The details of these blocks are described as follows.

Plain Block. This block is composed of the widely adopted ReLU-Conv2d-BatchNorm combo as in [1,13] with kernel size (3, 3), stride (1, 1), and padding size (1, 1). We place this type of block at the earlier stages of the network.

Downsample Block. This block consists of a Conv2d with stride (1, 2) in earlier stages and stride (2, 2) in later stages as in [46]. This is to retain the details in the vertical direction at earlier stages since the height h is much smaller than the width w . A BatchNorm unit is placed after the strided Conv2d for normalizing mini-batch statistics.

Residual Block. This block contains several ReLU-Conv2d-BatchNorm units with skip-connections [28] that sum up the inputs with the processed feature maps for residual learning. This has been proven conducive for the convergence of the network.

Upsample Block. This block first squeezes the channel dimensions for the given feature maps from the last four stages to C (the total number of classes) via 1×1 convolutions and then applies “deconvolutions” [39] for upsampling. The upsampled feature maps are then added together as a multi-scale feature aggregation.

Summary. Our segmentation network \mathcal{G} has a fully-convolutional structure [39] consisting of multiple stages for feature extraction and aggregation. At every stage, we expand the channel dimensions while reducing the width (at stages S1 to S7) and height (at stage S7) by a factor of 2. The reduction rates for the width w and height h are 64 and 2, respectively. The final prediction maps are composed of the sum of the upsampled feature maps from the last four stages. \mathcal{G} contains 38.81M parameters in total and can operate under around 471 GFLOPs.

Comparisons with Other Backbones. As mentioned in the main paper (*cf.* Sec. 3.1), our segmentation network \mathcal{G} offers better segmentation accuracy and inference speed. Specifically, we compare \mathcal{G} with state-of-the-art LiDAR segmentation backbones in Tab. 9. It can be seen that our network provides the best segmentation performance (in terms of mIoU scores) and also maintains promising computational speed (in terms of frame-rate). This builds a solid foundation for LiDAR domain adaptations since methods based on both adversarial training and self-training require accurate and efficient feature extractions. In this work, all UDA algorithms are sharing the same range-view segmentation backbone to ensure fair comparisons for their adaptation performance.

7.3 Anti-Aliasing Regularizer

As shown in Fig. 10, our proposed anti-aliasing (AA) regularizer (*cf.* Sec. 3.3) operates within each of the convolution blocks by modulating the weights of the convolution kernel \mathbf{f}_c with our learnable kernel \mathbf{f}_r , *i.e.*,

$$\mathbf{f}_{c,r} = \mathbf{f}_r \odot \mathbf{f}_c, \quad (6)$$

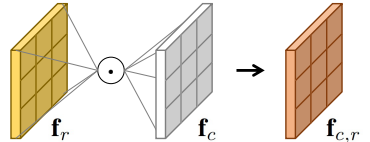
where \odot denotes the Hadamard multiplication; $\mathbf{f}_{c,r}$ is the regularized filter kernel which is then used for computation with the convolution input \mathbf{a}_c via $\mathbf{f}_{c,r} * \mathbf{a}_c$.

Based on previous observations [8,63] that the convolutional networks tend to learn low-frequency representations at earlier stages of training, the modulating

Table 9. Comparison among different LiDAR segmentation backbones on SemanticKITTI [5] *test* set. The models are grouped, from top to bottom, as point-based backbones, bird’s eye view (BEV) backbones, and range-view (RV) backbones. All IoU scores are given in percentage. Best score for each class is highlighted in **bold**. Symbol * denotes our implementation or results collected from public checkpoints.

Model	mIoU	car	bicy	moto	truck	o.veh	ped	b.cyc	m.cyc	road	park	walk	o.gro	build	fence	veg	trunk	terr	pole	sign	FPS
PointNet [53]	14.6	46.3	1.3	0.3	0.1	0.8	0.2	0.2	0.0	61.6	15.8	35.7	1.4	41.4	12.9	31.0	4.6	17.6	2.4	3.7	2
PointNet++ [54]	20.1	53.7	1.9	0.2	0.9	0.2	0.9	1.0	0.0	72.0	18.7	41.8	5.6	62.3	16.9	46.5	13.8	30.0	6.0	8.9	0.1
SPG [35]	17.4	49.3	0.2	0.2	0.1	0.8	0.3	2.7	0.1	45.0	0.6	28.5	0.6	64.3	20.8	48.9	27.2	24.6	15.9	0.8	0.2
SPLATNet [65]	22.8	66.6	0.0	0.0	0.0	0.0	0.0	0.0	0.0	70.4	0.8	41.5	0.0	68.7	27.8	72.3	35.9	35.8	13.8	0.0	-
LatticeNet [59]	52.9	92.9	16.6	22.2	26.6	21.4	35.6	43.0	46.0	90.0	59.4	74.1	22.0	88.2	58.8	81.7	63.6	63.1	51.9	48.4	-
S-BKI [21]	51.3	83.8	30.6	43.0	26.0	19.6	8.5	3.4	0.0	92.6	65.3	77.4	30.1	89.7	63.7	83.4	64.3	67.4	58.6	67.1	-
RandLA-Net [31]	53.9	94.2	26.0	25.8	40.1	38.9	49.2	48.2	7.2	90.7	60.3	73.7	20.4	86.9	56.3	81.4	61.3	66.8	49.2	47.7	22
<hr/>																					
PolarNet [94]	54.3	93.8	40.3	30.1	22.9	28.5	43.2	40.2	5.6	90.8	61.7	74.4	21.7	90.0	61.3	84.0	65.5	67.8	51.8	57.5	-
<hr/>																					
SSegV1 [80]	29.5	68.8	16.0	4.1	3.3	3.6	12.9	13.1	0.9	85.4	26.9	54.3	4.5	57.4	29.0	60.0	24.3	53.7	17.5	24.5	90
SSegV2 [81]	39.7	81.8	18.5	17.9	13.4	14.0	20.1	25.1	3.9	88.6	45.8	67.6	17.7	73.7	41.1	71.8	35.8	60.2	20.2	36.3	83
SSegV3 [83]	55.9	92.5	38.7	36.5	29.6	33.0	45.6	46.2	20.1	91.7	63.4	74.8	26.4	89.0	59.4	82.0	58.7	65.4	49.6	58.9	6
TDLNet [16]	37.6	81.5	29.4	19.6	6.6	6.5	23.7	20.1	2.4	85.8	8.7	59.3	1.0	78.6	39.6	77.1	46.0	58.1	32.6	39.1	-
TGConv [68]	40.9	90.8	2.7	16.5	15.2	12.1	23.0	28.4	8.1	83.9	33.4	63.9	15.4	83.4	49.0	79.5	49.3	58.1	35.8	28.5	0.3
RGNet21 [46]	47.4	85.4	26.2	26.5	18.6	15.6	31.8	33.6	4.0	91.4	57.0	74.0	26.4	81.9	52.3	77.6	48.4	63.6	36.0	50.0	25
RGNet53 [46]	49.9	85.3	22.7	33.6	25.8	22.2	36.8	31.4	4.7	91.7	65.1	74.0	28.2	82.9	54.8	77.3	50.0	64.6	39.1	52.3	13
RGNet++ [46]	52.2	91.4	25.7	34.4	25.7	23.0	38.3	38.8	4.8	91.8	65.0	75.2	27.8	87.4	58.6	80.5	55.1	64.6	47.9	55.9	12
SalsaNet [1]	45.4	87.5	26.2	24.6	24.0	17.5	33.2	31.1	8.4	89.7	51.7	70.7	19.7	82.8	48.0	73.0	40.0	61.7	31.3	41.9	-
SalsaNext [13]	59.5	91.9	48.3	38.6	38.9	31.9	60.2	59.0	19.4	91.7	63.7	75.8	29.1	90.2	64.2	81.8	63.6	66.5	54.3	62.1	-
3D-MiniNet [3]	55.8	90.5	42.3	42.1	28.5	29.4	47.8	44.1	14.5	91.6	64.2	74.5	25.4	89.4	60.8	82.8	60.8	66.7	48.0	56.6	28
FIDNet* [96]	58.6	93.0	45.7	42.0	27.9	32.6	62.6	58.1	30.5	90.8	58.3	74.9	20.1	88.5	59.5	83.1	64.3	67.8	52.6	60.0	-
Ours	59.6	90.4	31.9	57.6	79.8	45.7	61.9	64.9	0.0	95.3	48.9	81.8	8.0	85.3	59.7	84.1	58.8	69.9	53.4	44.7	19

Fig. 10. Illustration for the proposed anti-aliasing regularization (*cf.* Sec. 3.3). Our regularizer \mathbf{f}_r imposes regularization on high-frequency representations of the convolution filter \mathbf{f}_c via $\mathbf{f}_{c,r} = \mathbf{f}_r \odot \mathbf{f}_c$. The regularized filter kernel $\mathbf{f}_{c,r}$ is then used for the convolution computation.



regularizer \mathbf{f}_r will tend to become more correlated to low-frequency representation learning at such stages [93,99]. The gradient update corresponding to high-frequency aliasing-artifact representations will likely contain low correlations with the regularizer \mathbf{f}_r . Such low correlations between \mathbf{f}_r and the back-propagated gradient attenuate the influence of the high-frequency detrimental effect [73] and therefore regularize the network to such aliasing artifacts during the pre-training and self-training.

Comparing the frequency spectrum of 3x3 kernels from the network trained *w/* and *w/o* AA regularizer, we find that the ratio of ‘average low-frequency amplitudes’ to ‘average high-frequency amplitudes’ is 23.2% higher (statistically significant with t-test: $p < 0.001$) for the network trained with our AA regularizer. We also visualize (see Fig. 11) that kernels trained with AA regularizer tend to become closer to *low-pass filters*, hence better suppress high-frequency aliasing artifacts during UDA.

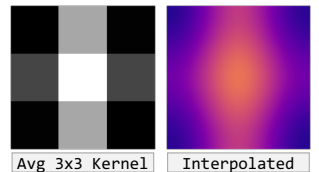


Fig. 11. Frequency spectrum of AA-regularized kernels. Left: discrete form; Right: continuous form.

Table 10. The complete (class-wise) adaptation results for different range-view concatenation strategies and other mixing techniques (*cf.* Tab. 3). All IoU scores are given in percentage. The best score for each semantic class is highlighted in **bold**.

Method	barr	bicy	bus	car	const	moto	ped	cone	trail	truck	driv	othe	walk	terr	mann	veg	FIoU	mIoU
w/o	42.6	4.6	67.5	73.2	10.1	23.1	51.4	14.0	0.0	39.3	88.1	24.9	38.1	56.0	66.8	70.5	70.0	41.9
a	43.9	4.9	69.4	74.4	12.2	30.1	53.1	15.1	0.0	40.7	88.3	28.4	38.9	55.6	67.8	71.7	70.5	43.4
b	43.1	5.5	68.3	74.5	11.6	31.6	52.5	15.1	0.0	40.2	88.8	29.5	38.7	58.0	67.8	71.2	70.9	43.5
c	45.0	5.2	69.8	75.2	12.0	29.6	52.7	15.7	0.0	41.5	88.1	30.2	38.8	55.3	68.2	72.1	70.6	43.7
d	49.8	4.7	68.2	75.0	12.4	27.7	50.3	15.8	0.0	39.3	89.7	39.3	41.0	57.3	68.7	72.7	71.9	44.5
e	50.2	4.8	68.8	75.9	12.8	30.4	52.4	15.7	0.0	41.0	88.7	33.2	41.0	60.0	67.8	71.0	71.5	44.6
f	45.1	4.4	68.0	75.4	11.4	28.5	52.6	15.7	0.0	42.5	88.3	34.0	38.7	58.5	67.7	71.5	71.0	43.9
g	47.6	5.8	69.9	75.0	11.6	28.2	51.6	15.8	0.0	43.0	89.4	36.0	40.3	57.8	68.2	71.9	71.6	44.5
h	49.7	5.1	70.3	75.2	12.4	27.3	52.1	16.0	0.0	41.0	89.0	33.1	41.2	59.7	68.6	72.6	72.0	44.6
i	49.6	6.7	71.1	75.0	13.7	30.3	52.8	16.0	0.0	40.3	90.0	36.0	42.0	60.0	68.8	72.9	72.6	45.3
j	51.0	5.6	68.7	75.5	12.9	27.4	52.3	15.8	0.0	41.0	90.0	35.9	42.6	60.3	68.6	72.6	72.5	45.0
k	49.6	7.2	68.4	75.3	11.8	29.9	52.8	15.5	0.0	42.6	89.9	36.1	43.4	58.6	69.2	73.8	72.6	45.2
l	52.6	6.4	70.2	77.2	11.9	25.6	51.8	15.2	0.0	43.4	90.7	38.6	42.1	57.5	68.6	72.6	72.4	45.3
m	48.6	4.8	70.9	76.2	12.5	27.9	51.9	15.4	0.0	42.2	90.9	33.1	42.4	58.4	69.3	73.4	72.8	44.9
n	46.1	4.3	69.3	76.6	11.8	23.9	51.8	16.5	0.0	40.6	90.5	38.3	43.1	60.0	68.4	72.3	72.6	44.6
o	49.2	5.1	67.1	74.9	12.4	26.9	51.7	15.9	0.0	40.2	89.2	33.5	41.8	57.7	68.8	72.7	71.8	44.2
SimROD [56]	23.2	1.4	40.1	64.0	8.1	1.9	43.0	8.6	0.0	28.0	85.4	18.8	34.7	51.7	63.9	65.9	66.0	33.7
MixUp [92]	44.1	2.7	66.7	73.2	10.4	20.4	47.9	12.6	0.0	37.1	88.0	32.1	38.8	55.1	63.6	64.5	68.0	41.1
CutOut [15]	41.5	6.6	68.7	72.4	10.8	29.9	52.3	14.6	0.0	38.2	88.5	30.3	38.4	55.3	67.8	72.4	70.6	43.1
CutMix [91]	39.6	4.0	67.0	72.0	11.2	27.3	52.4	16.3	0.0	40.0	88.7	33.7	39.1	52.6	66.9	70.5	69.7	42.6

8 Complete Results

8.1 Class-Wise Quantitative Results

We provide the complete results (class-wise IoU scores) for our ablation studies (*cf.* Tab. 3) in Tab. 10 and more discussions for Tab. 1. As can be seen from the ablative analysis in Tab. 1, the three proposed components bring overt improvements over the source-only case and the baseline. We observe that while the anti-aliasing regularizer tends to improve the adaptation results for static classes like ‘barrier’, ‘terrain’, and ‘vegetation’, the domain concatenation strategy brings significant gains for almost all semantic classes. On top of domain concatenation, the entropy aggregator further provides another holistic boost. This strongly supports our findings that mixing domains properly and regularizing aliasing artifacts and false target predictions are conducive for the adaptations. From Tab. 10 we find that as the granularity of the interactions between domains increases in a certain range, the adaptation results for almost all semantic classes are improved. The other mixing techniques [56,92,15,91], however, cannot maintain the spatial layouts or semantic consistency, thus bringing no or limited improvements over the baseline.

8.2 Visualizations for Running Statistics

During training, strong data augmentation like CutOut [15] and MixUp [92] tends to cause large distribution disparity due to its negative effect on the running statistics (*e.g.*, batch normalization (BN) statistics) [89,20,49]. To illustrate

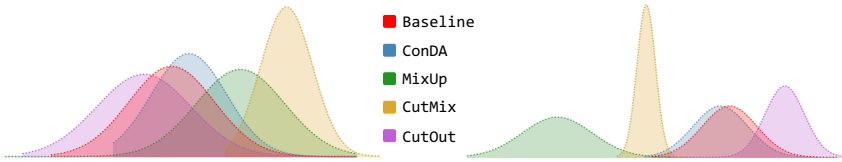


Fig. 12. Histogram of running *mean* (left) and *variance* (right) during self-training.

the impact of our range-view concatenation idea to these statistics, we calculate and visualize the running mean and variance from the BN layers during network self-training in Fig. 12. Specifically, we find that ConDA is not likely to cause problems to the running statistics, since: 1) self-training starts with pre-trained weights and small learning rate hence is relatively stable; 2) ConDA re-groups stripes instead of noising, jittering, or erasing. Compared to other mixing techniques, the BN statistics of ConDA are closest to that of the baseline. This verifies that our proposed methods can better maintain the running stability.

8.3 Additional Qualitative Results

We provide the qualitative results for our ablation studies (*cf.* Tab. 1) in Fig. 13 and additional qualitative results for our comparative studies (*cf.* Fig. 5) in Fig. 14 and Fig. 15. As can be seen from these visualizations, the street scenes (from the ground-truth views) often contain complex layouts with various types of semantic classes scattered around the ego-vehicle. While the previous arts [76,100,50] can only mitigate the false predictions of some classes in certain areas, ConDA provides convincing improvements in most regions for both dynamic and static classes, which demonstrates the effectiveness of our proposed approach in tackling domain adaptations for LiDAR segmentation.

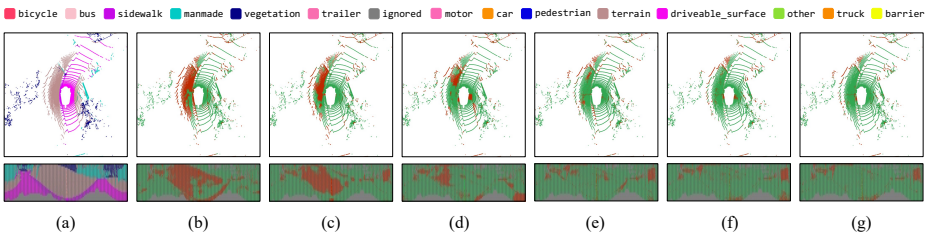


Fig. 13. Qualitative examples for the ablation results (*cf.* Table 1) from both the bird’s eye view and range-view. (a) Ground-truth. (b) No adaptation (source-only). (c) Baseline. (d) += Anti-aliasing regularizer. (e) += Domain concatenation. (f) += Entropy aggregator (round 1). (g) Full ConDA framework. To highlight the difference between the predictions and the ground-truth, the **correct** and **incorrect** points/pixels are painted in **green** and **red**, respectively. Best viewed in color.



Fig. 14. Additional qualitative results (1/2) from both the bird's eye view and range-view. To highlight the difference between the predictions and ground-truth, the **correct** and **incorrect** points/pixels are painted in **green** and **red**, respectively. Best viewed in color.



Fig. 15. Additional qualitative results (2/2) from both the bird's eye view and range-view. To highlight the difference between the predictions and ground-truth, the **correct** and **incorrect** points/pixels are painted in **green** and **red**, respectively. Best viewed in color.

9 Semi- & Weakly-Supervised Domain Adaptation

9.1 Semi-Supervised Domain Adaptation (SSDA)

Definition. As stated in the main paper, a more practical scenario for cross-city domain adaptation is to acquire a small set of labeled target data for the target domain with an acceptable budget. To formulate this SSDA setting, we uniformly sampled certain target samples and assume they are annotated.

Data Split. The detailed quota for the number of target samples with labels is shown in Tab. 11. More concretely, we uniformly sample 0.1%, 1%, 10%, 20%, 50% of the Boston/Singapore target samples and assign ground-truth annotations to them. The remaining target samples are kept unlabeled. Other configurations are the same as that of the UDA setting.

Results. We provide the complete results (class-wise IoU scores) for the SSDA studies (*cf.* Tab. 6) under 0.1%, 1%, 10%, 20%, 50% quota in Tab. 12, Tab. 13, Tab. 14, Tab. 15, and Tab. 16, respectively. It can be seen that the adaptation results can be overtly improved by involving certain labeled target samples. Such improvements are applicable for all the UDA methods [72,75,76,100] tested, and are especially large with our proposed domain concatenation idea. For example, with only 1% (124/156) labeled Singapore/Boston samples, ConDA can achieve 53.8%/51.6% mIoU, which is 18.9%/17.7% mIoU higher than the source-only results. If 20% labeled target samples are available, the adaptation results can be significantly improved (65.3% mIoU for Boston \rightarrow Singapore and 65.5% mIoU for Singapore \rightarrow Boston), which are close to that of the oracle results (65.8% and 67.3%, respectively). We are able to surpass the oracle results with 50% labeled target samples, which verifies that ConDA can bring strong augmentation and regularization capabilities during adaptations. Since SSDA shares some similarities with semi-supervised semantic segmentation, we also compared ConDA with state-of-the-art methods from this line, *i.e.*, MeanTeacher [67] and CPS [10]. Note that although such methods can improve the low-data scenarios where labeled and unlabeled groups share the same distribution, they are suffered from the domain gap and thus cannot achieve a good performance in SSDA. This finding further highlights the importance of considering domain discrepancy mitigation for cross-city deployment.

Table 11. Data split for SSDA. Certain proportions (%) of target samples are uniformly selected and assumed labeled. The rest target samples remain unlabeled. Left-half: splits for **Boston** \rightarrow **Singapore**; Right-half: splits for **Singapore** \rightarrow **Boston**.

Setting	Source Target	+0.1%	+1%	+10%	+20%	+50%	Source Target	+0.1%	+1%	+10%	+20%	+50%		
#Labeled samples	15695	12435	+12	+124	+1243	+2487	+6217	12435	15695	+15	+156	+1569	+3139	+7847

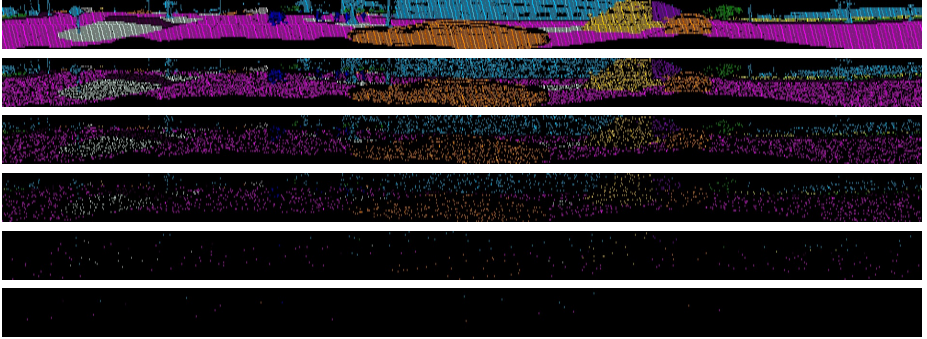


Fig. 16. Illustrative examples for the WSDA setting. **Row 1:** full supervision; **Row 2:** 50% semantic points; **Row 3:** 20% semantic points; **Row 4:** 10% semantic points (~ 2500 labeled points); **Row 5:** 1% semantic points (~ 250 labeled points); **Row 6:** 0.1% semantic points (~ 25 labeled points). Sample adopt from nuScenes [7]. The range-view resolution is set as 32×1920 . Best viewed in color.

9.2 Weakly-Supervised Domain Adaptation (WSDA)

Definition. Different from SSDA, WSDA assumes that all target training samples are partially annotated. Given a LiDAR point cloud, only a certain proportion of points inside this cloud are assumed labeled (*i.e.*, with semantic labels), and other points are unlabeled. Fig. 16 gives an example for this setting.

Data Split. We uniformly sample 0.1%, 1%, 10%, 20%, 50% annotated points from the Boston/Singapore target LiDAR point clouds and assign semantic annotations to them. Note that this procedure is done before the range-view projection. We do this to ensure that each LiDAR point cloud could maintain a relatively equal number of semantic points. The remaining target points are kept unlabeled (we assign *ignored label* to them, which corresponds to semantic label 255). Other configurations are the same as that of the UDA setting.

Results. We provide the complete results (class-wise IoU scores) for the WSDA studies (*cf.* Tab. 7) under 0.1%, 1%, 10%, 20%, 50% quota in Tab. 17, Tab. 18, Tab. 19, Tab. 20, and Tab. 21, respectively. Since there already exist partial labels, we do not generate pseudo-labels but directly concatenate the source samples (with full supervisions) with the target samples (with partial supervisions) during self-training. We find that such a sparse way of annotation can achieve very good segmentation results. Since a single LiDAR point cloud contains thousands of points, a partial (*e.g.* 10%) annotation has already provided sufficient supervision signals. As a concrete example, ConDA can achieve 55.9%/52.9% mIoU with only 0.1% Singapore/Boston point-level annotations. If we can label 10% points for each collected target LiDAR point cloud, we can obtain adaptation results which are as good as the oracle results (65.9% mIoU for Boston \rightarrow Singapore and 68.6% mIoU for Singapore \rightarrow Boston). All the mentioned results are in line with our findings in the main paper, which bring strong evidence to support ConDA’s augmentation and regularization capabilities under various scenarios.

Table 12. The complete (class-wise) adaptation results under SSDA setting with 0.1% labeled target data (*cf.* Table 6). Upper-half: results for **Boston** \rightarrow **Singapore**; Bottom-half: results for **Singapore** \rightarrow **Boston**. All IoU scores are given in percentage. The best score for each semantic class is highlighted in **bold**.

Method	barr	bicy	bus	car	const	moto	ped	cone	trail	truck	driv	othe	walk	terr	manm	veg	FIoU	mIoU
MeanTeacher [67]	3.3	0.0	6.8	27.4	0.2	0.0	8.7	2.4	0.0	13.5	18.9	0.4	14.9	0.4	3.6	27.6	14.7	7.8
CPS [10]	2.3	0.1	9.6	40.0	0.4	0.6	45.5	15.3	0.0	3.8	65.8	27.8	0.2	28.3	34.5	0.2	33.1	17.1
AdaptSeg [72]	36.5	6.3	67.8	76.7	6.1	7.8	54.7	21.8	0.0	33.7	87.3	37.1	34.5	38.2	65.1	71.0	66.5	40.3
MinEnt [75]	28.8	1.4	68.4	75.7	4.7	4.7	59.0	21.9	0.0	36.4	85.6	35.6	35.1	41.0	66.2	72.0	66.8	39.8
AdvEnt [75]	40.3	6.6	72.1	76.2	5.3	5.9	60.5	24.1	0.0	40.3	87.2	35.7	36.5	36.6	66.7	73.2	67.2	41.7
DADA [76]	37.6	4.9	68.2	77.7	3.4	6.0	56.9	20.7	0.0	39.6	86.9	33.2	34.9	35.2	65.6	71.8	66.3	40.2
CBST [100]	46.3	0.1	77.4	82.5	9.0	7.0	64.8	24.3	0.0	49.3	87.3	35.4	38.5	53.4	70.8	76.7	71.8	45.2
ConDA (Ous)	53.5	1.5	81.8	84.2	12.4	13.5	65.8	25.5	0.0	51.5	89.4	41.8	42.2	56.1	71.8	77.8	73.7	48.1
MeanTeacher [67]	28.7	0.0	20.9	65.0	0.1	0.0	21.5	7.3	0.4	31.2	80.5	0.0	34.4	0.8	33.5	29.7	53.5	22.1
CPS [10]	0.6	0.6	1.3	69.7	0.6	0.1	45.4	7.2	0.0	32.3	89.6	43.3	47.8	1.8	74.0	70.1	72.2	30.3
AdaptSeg [72]	11.0	8.3	50.2	76.7	7.5	9.2	57.7	10.8	0.0	48.4	95.1	24.2	60.1	24.1	81.1	77.0	78.5	40.0
MinEnt [75]	16.8	8.4	47.4	72.7	4.8	8.1	52.8	12.6	0.0	46.4	95.1	29.8	60.8	24.6	81.3	74.4	78.4	39.6
AdvEnt [75]	10.9	8.4	51.0	75.6	3.8	11.5	56.7	10.7	0.4	46.8	93.2	22.7	60.6	23.8	81.1	76.2	78.4	39.6
DADA [76]	10.3	7.7	48.3	72.8	7.0	10.1	55.1	11.9	0.1	45.7	93.3	27.6	60.6	23.8	81.1	75.9	78.3	39.5
CBST [100]	10.0	6.4	47.8	74.9	3.9	12.6	57.0	15.9	0.9	47.6	93.0	32.8	61.2	26.2	82.6	81.8	79.3	40.9
ConDA (Ous)	11.6	6.3	51.2	75.2	7.4	13.6	59.6	17.3	0.5	48.2	93.7	34.5	64.6	27.7	83.2	82.2	80.3	42.5

Table 13. The complete (class-wise) adaptation results under SSDA setting with 1% labeled target data (*cf.* Table 6). Upper-half: results for **Boston** \rightarrow **Singapore**; Bottom-half: results for **Singapore** \rightarrow **Boston**. All IoU scores are given in percentage. The best score for each semantic class is highlighted in **bold**.

Method	barr	bicy	bus	car	const	moto	ped	cone	trail	truck	driv	othe	walk	terr	manm	veg	FIoU	mIoU
MeanTeacher [67]	0.2	0.0	21.5	38.4	0.0	0.0	25.9	4.2	0.0	10.1	43.8	4.2	5.6	2.3	51.7	65.4	39.3	17.1
CPS [10]	6.8	0.7	7.5	76.0	0.7	0.5	58.4	16.0	0.0	38.9	89.2	14.7	27.8	29.7	49.9	54.5	58.4	29.5
AdaptSeg [72]	44.5	1.7	69.2	79.2	4.4	8.0	62.0	22.9	0.0	41.0	91.3	42.4	44.1	58.6	72.4	77.8	74.7	45.0
MinEnt [75]	49.9	1.6	73.8	77.0	5.8	8.8	63.0	24.2	0.0	40.9	89.8	39.9	42.2	59.0	71.9	76.9	73.8	45.3
AdvEnt [75]	47.2	1.8	74.7	79.7	3.6	8.9	62.5	23.8	0.0	43.8	91.0	43.0	44.3	60.4	73.3	77.5	75.1	46.0
DADA [76]	42.8	1.5	71.4	79.9	3.8	7.7	61.3	25.7	0.0	43.9	90.8	43.9	44.4	59.2	71.9	76.9	74.4	45.3
CBST [100]	54.5	0.5	81.5	82.2	8.8	23.4	66.2	29.5	0.0	54.3	92.4	51.6	51.1	70.3	76.9	80.7	79.2	51.5
ConDA (Ous)	56.8	1.5	83.0	85.4	8.6	28.7	67.2	34.1	0.0	57.4	93.3	56.6	54.3	72.2	78.4	82.5	80.9	53.8
MeanTeacher [67]	22.9	0.0	15.8	62.2	0.3	0.0	35.0	23.3	6.0	4.8	54.8	35.3	36.6	0.2	51.3	42.4	47.6	24.4
CPS [10]	7.3	0.4	2.5	69.7	0.5	6.3	48.6	10.9	0.0	36.7	87.7	48.2	47.8	17.1	73.0	55.5	70.7	32.0
AdaptSeg [72]	30.4	6.4	50.4	75.6	14.2	12.2	57.9	44.4	17.0	45.9	96.3	36.1	66.6	30.0	83.2	78.0	80.9	45.9
MinEnt [75]	35.3	8.0	50.9	75.7	12.3	14.9	53.4	42.9	19.6	48.1	96.5	37.1	66.6	31.5	83.8	78.0	81.0	47.0
AdvEnt [75]	36.6	4.1	51.1	78.3	9.7	12.9	61.9	41.9	12.1	47.8	93.6	36.3	64.9	31.2	83.7	77.6	80.8	46.5
DADA [76]	34.4	9.3	49.9	73.0	6.1	11.8	58.1	41.3	18.5	46.1	94.1	36.7	66.6	29.1	82.8	75.6	80.5	45.8
CBST [100]	40.8	8.5	50.1	72.9	11.0	17.3	61.7	50.4	22.5	45.9	94.4	46.7	70.5	34.7	85.3	82.0	82.5	49.7
ConDA (Ous)	44.7	12.5	48.4	74.1	13.3	30.2	63.9	55.5	23.9	44.5	94.7	44.7	71.9	35.3	86.2	82.4	83.1	51.6

Table 14. The complete (class-wise) adaptation results under SSDA setting with 10% labeled target data (*cf.* Table 6). Upper-half: results for **Boston** \rightarrow **Singapore**; Bottom-half: results for **Singapore** \rightarrow **Boston**. All IoU scores are given in percentage. The best score for each semantic class is highlighted in **bold**.

Method	barr	bicy	bus	car	const	moto	ped	cone	trail	truck	driv	othe	walk	terr	manm	veg	FIoU	mIoU
MeanTeacher [67]	0.9	0.0	45.0	53.2	2.6	0.8	21.2	12.9	0.0	8.6	74.2	25.8	22.5	58.0	47.0	38.3	53.0	25.7
CPS [10]	54.4	0.0	37.6	66.0	1.3	1.6	61.9	17.5	0.0	23.5	86.6	45.2	23.4	63.9	58.4	70.1	67.8	38.2
AdaptSeg [72]	64.7	8.0	80.9	85.2	18.2	22.4	67.3	36.3	0.0	56.1	93.6	58.0	54.8	71.9	79.3	82.6	81.2	55.0
MinEnt [75]	64.6	7.6	83.5	83.5	18.8	27.5	66.4	36.2	0.0	56.9	93.2	54.2	53.3	71.3	78.6	82.0	80.5	54.9
AdvEnt [75]	64.7	6.8	82.7	84.9	22.3	25.4	66.8	35.5	0.0	58.4	93.5	56.0	55.0	72.3	78.9	82.3	81.1	55.4
DADA [76]	64.3	10.1	78.5	83.3	19.1	24.5	66.6	35.0	0.0	52.3	93.5	55.3	54.1	71.4	78.1	81.8	80.5	54.2
CBST [100]	71.1	7.9	88.3	86.7	20.3	38.7	70.2	44.6	0.0	67.3	94.6	59.2	59.0	74.5	81.6	84.5	83.2	59.3
ConDA (Ous)	75.8	20.5	88.4	88.4	23.1	64.1	70.5	45.2	0.0	69.2	94.8	59.2	60.7	74.9	82.2	85.1	83.8	62.6
MeanTeacher [67]	49.7	8.5	10.6	78.3	9.9	0.6	67.7	60.4	25.3	37.1	94.3	65.4	65.3	22.8	85.2	80.5	81.9	47.6
CPS [10]	38.6	0.2	21.0	72.4	4.4	0.0	55.7	30.6	12.6	36.6	90.9	63.2	57.2	26.0	79.2	76.0	77.3	41.5
AdaptSeg [72]	59.3	25.0	60.4	81.6	25.7	17.4	65.4	57.2	36.8	57.5	97.1	56.9	73.5	49.5	87.5	82.5	85.4	58.2
MinEnt [75]	58.9	27.3	58.1	79.4	29.4	22.5	64.9	58.5	34.8	54.8	97.6	60.4	76.4	51.0	87.5	83.4	85.9	58.9
AdvEnt [75]	59.2	30.1	61.7	82.8	27.0	24.2	64.8	58.5	38.8	59.6	95.2	61.1	73.7	50.5	87.6	82.7	85.8	59.8
DADA [76]	60.3	28.7	58.1	84.0	25.2	21.0	65.6	59.5	37.3	59.0	95.3	59.4	61.3	49.8	87.3	82.3	85.8	59.2
CBST [100]	65.8	32.7	58.5	81.2	28.5	14.2	68.7	61.1	37.7	55.6	95.7	65.7	77.2	55.1	88.5	84.6	86.8	60.7
ConDA (Ous)	66.4	35.5	59.0	80.6	31.7	27.4	70.1	63.4	40.7	57.9	95.8	67.0	77.8	55.5	88.6	83.9	87.0	62.6

Table 15. The complete (class-wise) adaptation results under SSDA setting with 20% labeled target data (*cf.* Table 6). Upper-half: results for **Boston** \rightarrow **Singapore**; Bottom-half: results for **Singapore** \rightarrow **Boston**. All IoU scores are given in percentage. The best score for each semantic class is highlighted in **bold**.

Method	barr	bicy	bus	car	const	moto	ped	cone	trail	truck	driv	othe	walk	terr	manm	veg	FIoU	mIoU
MeanTeacher [67]	2.4	3.1	78.6	37.3	18.4	13.7	44.4	0.4	0.0	3.7	53.6	44.2	27.2	57.7	28.5	41.7	44.1	28.4
CPS [10]	44.1	0.0	63.7	84.0	9.5	3.5	67.3	22.1	0.0	62.8	90.3	56.7	25.8	66.1	63.3	72.9	71.7	45.8
AdaptSeg [72]	71.1	18.6	85.3	86.2	25.5	28.5	70.5	42.3	0.0	62.4	94.2	55.4	58.6	73.9	81.2	84.3	82.8	58.6
MinEnt [75]	72.4	16.8	85.9	86.9	27.2	39.9	69.7	40.2	0.0	63.8	94.2	54.7	57.7	73.1	81.3	84.4	82.7	59.3
AdvEnt [75]	72.0	17.5	85.9	86.7	29.5	44.3	69.4	39.0	0.0	61.2	94.2	56.6	57.0	72.2	80.4	83.5	82.1	59.4
DADA [76]	73.6	16.2	85.9	86.5	27.0	31.6	69.7	42.1	0.0	62.7	94.2	56.1	58.1	73.7	81.3	84.5	82.8	59.0
CBST [100]	77.3	19.6	87.7	87.4	31.0	41.9	71.1	48.0	0.0	70.4	94.7	56.0	60.0	74.7	82.5	85.3	83.8	61.7
ConDA (Ous)	78.6	26.3	90.1	89.1	35.6	40.9	71.8	49.4	0.0	73.8	94.9	58.6	61.4	75.6	82.8	85.5	84.3	65.3
MeanTeacher [67]	63.2	17.4	30.8	74.8	6.5	4.5	69.0	60.7	28.8	34.0	93.2	70.4	57.0	14.1	85.5	78.1	80.6	49.3
CPS [10]	62.5	16.7	52.1	81.0	14.9	3.0	66.5	54.5	30.4	50.7	95.9	70.9	76.8	53.8	86.2	81.6	85.8	56.1
AdaptSeg [72]	62.6	31.9	64.8	82.8	28.7	26.9	64.0	62.5	44.7	59.8	97.4	65.1	76.9	53.9	88.6	84.2	86.9	62.1
MinEnt [75]	64.2	31.9	62.9	84.1	23.8	29.5	66.4	61.5	41.0	60.8	97.7	63.6	77.4	53.4	88.5	83.9	87.0	61.8
AdvEnt [75]	62.8	32.9	65.2	84.7	28.3	21.9	64.7	62.4	46.9	62.3	95.5	65.7	76.1	53.8	88.6	84.1	87.0	62.2
DADA [76]	63.5	31.0	63.3	83.9	33.0	26.5	66.7	62.8	42.7	59.7	95.8	66.4	77.8	53.9	88.6	83.8	87.1	62.5
CBST [100]	64.3	34.2	64.3	84.6	31.2	14.5	70.0	65.3	47.6	62.0	95.7	67.2	78.0	57.6	89.3	85.1	87.6	63.2
ConDA (Ous)	66.2	33.6	67.0	84.5	36.0	33.2	71.5	66.0	49.4	64.6	96.1	70.5	79.6	56.6	89.1	84.2	88.0	65.5

Table 16. The complete (class-wise) adaptation results under SSDA setting with 50% labeled target data (*cf.* Table 6). Upper-half: results for **Boston** \rightarrow **Singapore**; Bottom-half: results for **Singapore** \rightarrow **Boston**. All IoU scores are given in percentage. The best score for each semantic class is highlighted in **bold**.

Method	barr	bicy	bus	car	const	moto	ped	cone	trail	truck	driv	othe	walk	terr	manm	veg	FIoU	mIoU
MeanTeacher [67]	3.2	4.4	66.1	66.6	9.1	3.2	40.4	46.9	0.0	19.6	78.5	33.5	22.5	69.3	68.3	72.0	67.8	37.7
CPS [10]	76.4	0.3	83.7	87.5	31.8	23.6	70.2	39.1	0.0	72.3	93.1	56.3	51.5	69.8	53.6	67.1	72.7	54.8
AdaptSeg [72]	78.3	29.7	89.7	88.9	31.3	47.6	72.4	48.5	0.0	71.6	95.0	53.8	60.0	73.7	82.8	85.5	83.9	63.1
MinEnt [75]	78.7	22.5	89.8	89.8	33.3	52.5	72.9	47.3	0.0	74.0	94.9	53.9	59.6	74.1	83.3	85.7	84.0	63.3
AdvEnt [75]	78.1	26.1	89.2	89.8	32.4	41.6	73.0	46.7	0.0	70.6	95.0	53.5	60.0	74.2	83.3	85.7	84.1	62.5
DADA [76]	78.3	29.0	90.5	89.4	29.5	35.3	73.0	46.9	0.0	71.1	94.8	55.4	59.0	73.5	83.0	85.5	83.8	62.2
CBST [100]	79.3	29.2	90.1	90.4	35.1	51.5	73.6	50.6	0.0	75.2	95.1	54.9	61.0	74.8	83.6	85.9	84.5	64.4
ConDA (Ous)	80.8	34.8	91.8	91.6	38.4	75.5	73.4	53.3	0.0	78.0	95.2	57.1	62.3	76.0	84.0	86.3	85.0	67.4
MeanTeacher [67]	70.6	28.1	68.1	83.0	25.2	2.9	70.4	65.3	53.9	61.7	95.2	71.7	71.8	37.5	88.9	84.0	86.4	61.2
CPS [10]	69.6	35.0	60.9	82.7	25.2	16.0	69.5	62.4	50.2	64.1	96.1	73.8	78.3	51.3	87.7	82.5	87.3	62.8
AdaptSeg [72]	69.7	39.4	72.4	85.8	36.5	30.3	66.4	66.0	56.1	68.2	98.0	69.7	80.2	59.1	90.0	85.4	88.7	66.9
MinEnt [75]	69.5	38.3	71.6	84.8	39.5	25.1	69.0	65.8	53.6	66.6	97.8	72.0	79.6	59.1	90.1	85.7	88.6	66.7
AdvEnt [75]	67.4	36.3	70.8	86.2	35.3	31.6	70.5	65.1	54.4	67.3	96.1	70.9	79.7	59.4	89.8	85.6	88.6	66.7
DADA [76]	69.7	35.0	71.8	86.6	39.2	33.4	72.3	65.7	58.0	69.2	96.2	70.1	80.0	58.4	89.8	85.2	88.7	67.5
CBST [100]	71.4	41.5	71.8	85.7	37.9	23.7	70.4	66.5	54.5	66.9	96.0	71.5	79.2	58.9	90.1	85.7	88.6	67.0
ConDA (Ous)	72.6	41.5	79.5	86.5	42.6	35.8	73.9	67.9	59.3	72.6	96.3	72.2	80.9	61.1	90.5	85.9	89.4	70.0

Table 17. The complete (class-wise) adaptation results under WSDA setting with 0.1% annotated target points per LiDAR point cloud (*cf.* Table 7). Upper-half: results for **Boston** \rightarrow **Singapore**; Bottom-half: results for **Singapore** \rightarrow **Boston**. All IoU scores are given in percentage. The best score for each semantic class is highlighted in **bold**.

Method	barr	bicy	bus	car	const	moto	ped	cone	trail	truck	driv	othe	walk	terr	manm	veg	FIoU	mIoU
Labeled-only	61.9	6.3	83.7	84.3	17.3	27.0	62.6	30.8	0.0	59.9	91.9	50.0	48.5	63.0	74.9	79.2	77.1	52.6
MeanTeacher [67]	57.3	9.6	73.6	85.4	17.8	40.8	57.9	30.4	0.0	57.8	91.7	52.8	51.8	69.5	76.1	80.3	78.8	53.3
CPS [10]	67.2	4.0	80.9	86.6	22.8	27.7	65.7	24.0	0.0	65.8	93.9	57.4	54.7	70.4	78.2	81.8	80.7	55.1
AdaptSeg [72]	63.1	4.8	85.8	84.1	18.1	26.8	62.8	30.1	0.0	62.8	92.2	49.2	50.8	65.5	74.4	78.7	77.6	53.1
MinEnt [75]	62.7	9.7	85.5	84.5	16.3	22.5	63.1	31.3	0.0	62.4	92.9	52.7	51.3	66.4	75.5	79.3	78.4	53.5
AdvEnt [75]	64.6	2.9	84.0	84.4	21.4	29.9	62.5	30.2	0.0	62.0	92.5	50.6	49.0	64.4	75.6	79.5	77.8	53.3
DADA [76]	65.7	8.7	83.2	85.3	21.7	23.1	63.0	31.5	0.0	63.2	92.7	50.9	50.5	63.8	74.9	78.7	77.6	53.6
ConDA (Ous)	68.8	10.1	86.7	86.0	21.5	35.2	64.8	34.9	0.0	66.0	93.0	51.3	52.6	67.1	75.9	79.7	78.9	55.9
Labeled-only	41.2	7.6	55.7	76.9	12.4	13.7	53.5	35.6	29.8	55.4	94.3	57.4	68.9	43.5	84.0	77.8	82.6	50.5
MeanTeacher [67]	55.2	7.2	54.4	73.6	23.1	14.0	55.8	44.7	24.3	51.5	94.5	61.1	71.5	43.0	85.1	77.7	83.2	52.3
CPS [10]	49.8	0.2	60.5	81.7	8.0	1.2	57.0	44.5	21.9	59.1	95.2	48.9	72.9	45.6	85.6	80.6	84.3	50.8
AdaptSeg [72]	43.3	14.8	58.7	79.6	18.1	12.1	58.3	38.9	23.2	57.6	94.5	52.1	71.0	40.5	84.6	79.5	83.2	51.7
MinEnt [75]	43.2	12.6	61.5	76.2	21.7	9.6	53.5	29.0	21.6	55.4	94.4	57.6	71.1	40.8	84.5	78.4	82.9	50.7
AdvEnt [75]	47.7	11.2	62.0	78.1	20.0	13.9	57.4	37.2	27.1	56.3	95.0	57.7	73.6	44.4	85.3	79.4	84.0	52.9
DADA [76]	36.7	11.5	61.7	81.6	23.0	14.9	56.3	40.2	22.5	58.4	93.8	52.2	68.6	40.9	84.7	80.0	82.8	51.7
ConDA (Ous)	49.9	17.3	57.9	80.5	26.1	19.6	63.2	30.1	25.2	57.5	94.7	47.7	70.9	38.8	85.4	81.4	83.7	52.9

Table 18. The complete (class-wise) adaptation results under WSDA setting with 1% annotated target points per LiDAR point cloud (*cf.* Table 7). Upper-half: results for **Boston** \rightarrow **Singapore**; Bottom-half: results for **Singapore** \rightarrow **Boston**. All IoU scores are given in percentage. The best score for each semantic class is highlighted in **bold**.

Method	barr	bicy	bus	car	const	moto	ped	cone	trail	truck	driv	othe	walk	terr	manm	veg	FIoU	mIoU
Labeled-only	73.7	14.0	88.3	88.1	30.4	46.2	69.6	41.7	0.0	70.5	94.2	49.5	55.1	69.2	79.6	82.7	81.2	59.6
MeanTeacher [67]	69.1	14.9	85.7	88.1	23.0	50.3	67.7	38.5	0.0	64.1	94.3	57.2	58.1	73.1	79.6	82.6	82.1	59.2
CPS [10]	78.4	4.5	89.1	89.5	32.6	34.2	72.1	23.4	0.0	75.1	94.7	59.2	58.5	73.9	81.8	84.6	83.3	59.5
AdaptSeg [72]	72.4	16.5	87.9	88.4	27.0	47.0	67.2	39.9	0.0	71.7	94.0	54.7	55.2	70.0	79.3	82.8	81.3	59.6
MinEnt [75]	73.4	18.9	88.6	88.6	27.4	41.7	69.1	41.8	0.0	73.2	94.3	51.2	55.9	70.0	80.0	83.0	81.6	59.8
AdvEnt [75]	73.6	13.9	87.1	88.2	25.2	44.4	68.7	40.9	0.0	70.6	93.8	51.4	54.3	69.2	79.1	82.0	80.8	58.9
DADA [76]	72.0	13.4	84.4	87.1	26.9	47.3	67.9	40.8	0.0	64.6	94.0	51.6	55.9	70.4	78.6	81.7	81.0	58.5
ConDA (Ous)	74.4	14.5	86.9	90.2	30.3	61.5	70.3	43.0	0.0	72.3	94.5	49.3	57.8	73.0	81.1	83.9	82.7	61.4
Labeled-only	59.9	28.1	68.7	84.1	31.9	17.7	65.7	42.7	36.1	64.7	96.0	58.8	77.4	52.7	88.2	83.6	86.9	59.8
MeanTeacher [67]	64.9	22.7	71.6	85.1	30.6	29.9	67.7	58.0	41.2	66.6	95.8	61.5	77.4	54.9	88.4	83.1	87.2	62.5
CPS [10]	60.6	18.8	78.4	85.0	26.6	30.0	71.5	57.2	49.1	69.2	95.9	61.4	78.0	53.0	88.5	83.8	87.4	62.9
AdaptSeg [72]	54.2	26.3	70.3	83.2	30.5	24.5	65.5	54.7	36.2	63.4	95.3	60.3	75.5	48.9	87.0	82.2	85.9	59.9
MinEnt [75]	59.3	22.1	74.6	84.0	29.4	21.5	65.6	44.0	38.3	65.3	95.8	60.9	76.9	51.0	88.1	83.4	86.8	60.0
AdvEnt [75]	58.4	29.0	70.4	83.1	24.7	27.0	66.1	47.9	35.7	62.4	95.7	55.1	76.3	50.3	87.8	83.4	86.3	59.6
DADA [76]	55.0	27.1	73.8	81.0	28.3	32.9	67.0	47.1	42.4	62.9	95.6	57.7	75.8	50.7	87.8	83.6	86.2	60.5
ConDA (Ous)	65.4	31.7	72.5	86.4	39.7	35.1	70.2	57.6	55.8	69.5	95.4	59.1	75.1	50.4	89.1	84.4	87.2	64.8

Table 19. The complete (class-wise) adaptation results under WSDA setting with 10% annotated target points per LiDAR point cloud (*cf.* Table 7). Upper-half: results for **Boston** \rightarrow **Singapore**; Bottom-half: results for **Singapore** \rightarrow **Boston**. All IoU scores are given in percentage. The best score for each semantic class is highlighted in **bold**.

Method	barr	bicy	bus	car	const	moto	ped	cone	trail	truck	driv	othe	walk	terr	manm	veg	FIoU	mIoU
Labeled-only	77.6	27.0	89.2	89.9	31.0	51.6	72.3	47.7	0.0	73.3	94.9	53.8	58.3	71.4	82.0	84.8	83.1	62.8
MeanTeacher [67]	76.4	30.1	89.0	89.5	28.6	49.8	72.1	44.7	0.0	70.7	94.9	56.6	59.2	73.0	82.2	84.9	83.4	62.6
CPS [10]	79.3	12.6	92.1	91.6	34.5	56.3	73.5	50.9	0.0	77.6	95.4	57.3	61.5	75.5	83.4	85.9	84.7	64.2
AdaptSeg [72]	77.3	25.4	89.5	90.0	29.0	45.6	71.7	47.0	0.0	72.7	94.4	51.7	55.9	69.5	81.0	83.7	82.0	61.5
MinEnt [75]	75.7	23.4	89.6	89.3	31.2	49.7	70.5	46.2	0.0	73.1	94.6	53.1	57.1	70.9	81.0	84.0	82.4	61.8
AdvEnt [75]	77.0	29.1	90.4	89.0	32.8	46.7	71.3	47.5	0.0	74.9	94.7	53.5	57.9	71.6	81.3	84.1	82.7	62.6
DADA [76]	77.4	24.3	90.5	89.8	29.0	46.5	72.6	48.3	0.0	73.4	94.8	52.8	57.9	72.9	81.8	84.4	83.1	62.3
ConDA (Ous)	79.3	32.5	91.5	91.0	37.3	68.8	72.6	49.5	0.0	73.8	95.2	56.6	61.7	76.0	83.4	86.0	84.7	65.9
Labeled-only	63.2	36.4	74.7	84.5	31.4	30.1	69.1	54.1	38.5	65.9	95.7	65.6	77.1	56.7	89.2	85.1	87.5	63.6
MeanTeacher [67]	63.4	30.9	73.3	85.4	37.0	39.4	72.1	56.0	50.8	69.8	95.7	62.6	77.5	54.9	89.6	85.4	87.8	65.2
CPS [10]	62.5	37.2	73.4	84.9	40.8	30.6	71.3	60.0	50.3	68.2	96.1	69.9	79.3	57.5	89.5	85.4	88.3	66.1
AdaptSeg [72]	62.1	29.0	73.7	84.9	38.3	21.5	66.8	54.7	34.6	65.5	95.2	65.4	75.8	52.8	88.0	82.7	86.6	61.9
MinEnt [75]	61.6	36.4	70.9	86.0	33.4	32.1	69.9	57.8	39.8	66.9	95.9	63.4	77.6	55.7	88.8	84.4	87.5	63.8
AdvEnt [75]	62.0	37.5	75.1	85.2	29.0	35.2	69.4	55.2	34.0	66.7	96.1	60.8	78.0	54.8	88.7	84.7	87.6	63.3
DADA [76]	57.3	34.9	70.9	86.8	24.5	30.2	69.7	55.2	36.1	67.3	95.7	63.7	77.6	54.8	88.4	84.1	87.3	62.3
ConDA (Ous)	71.5	39.7	80.8	86.3	35.9	40.9	70.2	65.2	58.4	72.0	96.1	69.6	79.4	57.6	89.9	84.5	88.7	68.6

Table 20. The complete (class-wise) adaptation results under WSDA setting with 20% annotated target points per LiDAR point cloud (*cf.* Table 7). Upper-half: results for **Boston** \rightarrow **Singapore**; Bottom-half: results for **Singapore** \rightarrow **Boston**. All IoU scores are given in percentage. The best score for each semantic class is highlighted in **bold**.

Method	barr	bicy	bus	car	const	moto	ped	cone	trail	truck	driv	othe	walk	terr	mann	veg	FIoU	mIoU
Labeled-only	78.0	31.7	88.0	89.3	29.9	49.2	72.3	46.8	0.0	71.5	94.7	52.9	58.3	72.0	81.8	84.5	82.9	62.6
MeanTeacher [67]	78.1	28.3	90.7	90.5	31.8	60.2	70.8	49.0	0.0	74.7	94.7	56.7	58.5	72.8	81.9	84.8	83.3	64.0
CPS [10]	79.3	26.5	91.3	91.0	34.5	55.3	73.8	50.3	0.0	78.6	95.2	58.3	61.0	74.7	82.9	85.5	84.3	64.9
AdaptSeg [72]	77.5	29.1	89.3	89.6	31.8	40.7	71.9	47.6	0.0	74.6	94.8	56.3	58.0	71.3	81.2	83.9	82.6	62.4
MinEnt [75]	77.7	27.7	90.5	89.2	30.8	40.8	72.4	49.9	0.0	75.2	94.4	53.5	56.4	70.2	81.2	84.0	82.3	62.1
AdvEnt [75]	77.4	29.5	90.5	89.5	29.5	49.8	72.2	46.9	0.0	74.9	94.8	53.4	58.0	72.5	81.7	84.3	83.0	62.8
DADA [76]	76.9	28.1	90.3	89.2	31.7	51.9	72.3	46.4	0.0	73.0	94.6	52.1	57.2	71.5	81.1	83.8	82.5	62.5
ConDA (Ours)	80.0	34.2	91.7	91.6	38.1	75.0	74.0	50.4	0.0	78.4	95.6	58.1	62.8	75.7	83.9	86.2	85.1	67.2
Labeled-only	62.5	31.1	75.5	85.8	33.2	32.9	71.8	57.4	41.6	67.1	95.6	64.1	75.9	57.0	89.4	85.3	87.5	64.1
MeanTeacher [67]	65.3	34.6	74.3	87.3	36.4	37.7	72.6	59.8	46.8	70.1	96.1	62.5	79.0	55.2	89.7	85.7	88.4	65.8
CPS [10]	66.0	24.6	78.2	87.8	37.8	35.3	73.5	58.7	55.6	74.1	96.3	61.8	80.0	57.3	90.0	85.4	88.8	66.4
AdaptSeg [72]	63.0	36.0	71.7	83.7	27.2	37.7	69.8	57.0	42.3	64.6	95.8	66.3	77.6	55.2	89.2	85.1	87.5	63.9
MinEnt [75]	64.2	35.0	77.0	84.6	32.0	28.7	70.6	59.1	41.0	66.6	96.1	68.8	79.1	57.1	88.9	84.6	88.0	64.6
AdvEnt [75]	60.2	39.4	73.5	87.0	30.6	37.2	70.7	53.9	35.9	69.2	95.9	63.0	77.5	55.1	88.9	84.6	87.6	63.9
DADA [76]	61.3	35.3	70.8	86.8	33.6	32.5	68.5	52.9	42.9	66.4	95.9	62.4	77.8	55.4	89.1	84.9	87.7	63.5
ConDA (Ours)	72.7	40.7	78.9	87.0	43.6	49.7	74.8	66.4	61.4	71.9	96.4	71.3	80.8	60.7	90.6	85.6	89.4	70.8

Table 21. The complete (class-wise) adaptation results under WSDA setting with 50% annotated target points per LiDAR point cloud (*cf.* Table 7). Upper-half: results for **Boston** \rightarrow **Singapore**; Bottom-half: results for **Singapore** \rightarrow **Boston**. All IoU scores are given in percentage. The best score for each semantic class is highlighted in **bold**.

Method	barr	bicy	bus	car	const	moto	ped	cone	trail	truck	driv	othe	walk	terr	mann	veg	FIoU	mIoU
Labeled-only	76.4	28.7	87.8	89.9	33.1	59.8	71.7	48.4	0.0	72.5	94.8	52.1	57.2	70.1	81.0	83.7	82.3	63.0
MeanTeacher [67]	80.4	28.3	91.4	90.6	34.5	51.5	74.2	50.2	0.0	75.8	95.3	55.6	61.2	74.3	83.5	85.8	84.4	64.5
CPS [10]	79.3	16.9	91.1	90.9	31.9	55.1	74.6	50.5	0.0	78.0	95.3	58.6	61.0	74.2	83.0	85.6	84.3	64.1
AdaptSeg [72]	78.1	27.6	90.8	89.6	29.5	45.2	72.6	49.2	0.0	75.9	94.7	55.1	58.8	73.2	80.6	83.5	82.8	62.8
MinEnt [75]	78.4	30.7	89.3	89.9	29.8	47.3	72.6	48.0	0.0	74.1	94.8	53.0	57.8	70.6	82.1	84.9	82.9	62.7
AdvEnt [75]	77.3	30.3	89.7	88.9	29.7	47.2	72.5	49.6	0.0	71.6	94.6	49.8	58.2	72.1	81.6	84.4	82.9	62.4
DADA [76]	77.7	27.0	91.5	90.2	35.7	52.9	72.6	48.5	0.0	74.3	94.8	53.9	57.1	72.4	82.0	84.8	83.1	63.5
ConDA (Ours)	81.9	37.0	92.3	91.8	38.5	66.4	74.1	53.1	0.0	78.8	95.7	57.3	63.0	75.8	84.1	86.4	85.3	67.3
Labeled-only	61.9	34.7	76.5	85.4	34.7	40.1	68.5	55.9	45.3	68.4	96.2	60.9	78.7	54.7	89.3	85.6	88.0	64.8
MeanTeacher [67]	63.9	34.1	74.8	86.2	37.0	43.5	72.6	59.7	45.3	68.3	96.2	61.1	79.4	56.3	89.6	85.8	88.3	65.9
CPS [10]	64.9	38.8	77.0	87.7	35.3	31.8	74.4	63.5	52.3	72.2	96.1	66.8	79.5	56.6	89.8	85.7	88.7	67.0
AdaptSeg [72]	60.6	35.8	78.2	87.3	30.0	35.9	71.0	55.9	42.3	70.6	96.2	64.4	79.3	55.7	89.1	84.8	88.2	64.8
MinEnt [75]	62.4	35.9	77.4	86.4	34.1	35.7	70.5	58.0	42.4	69.5	95.7	63.1	77.2	56.1	89.0	84.9	87.7	64.9
AdvEnt [75]	59.4	36.1	70.6	82.6	27.4	30.7	70.2	53.1	35.7	62.6	95.8	60.5	77.1	54.2	88.6	84.3	86.9	61.8
DADA [76]	63.1	33.1	72.8	85.7	34.6	34.7	67.2	57.3	37.5	66.0	95.6	63.7	76.0	55.8	88.9	84.7	87.3	63.6
ConDA (Ours)	72.8	42.8	80.3	88.3	44.0	50.8	75.1	66.9	62.7	73.8	96.6	68.6	82.2	59.9	90.7	86.2	89.8	71.4

References

1. Aksoy, E.E., Baci, S., Cavdar, S.: Salsanet: Fast road and vehicle segmentation in lidar point clouds for autonomous driving. In: IEEE Intelligent Vehicles Symposium. pp. 926–932 (2020) [6](#), [20](#), [21](#)
2. Alonso, I., Montesano, L.R., Murillo, A.C.: Domain adaptation in lidar semantic segmentation. arXiv preprint arXiv:2010.12239 (2020) [4](#)
3. Alonso, I., Riazuelo, L., Montesano, L., Murillo, A.C.: 3d-mininet: Learning a 2d representation from point clouds for fast and efficient 3d lidar semantic segmentation. IEEE Robotics and Automation Letters **5**(4), 5432–5439 (2020) [6](#), [21](#)
4. Araslanov, N., Roth, S.: Self-supervised augmentation consistency for adapting semantic segmentation. In: Proceedings of the IEEE/CVF Conference on Computer Vision and Pattern Recognition. pp. 15384–15394 (2021) [2](#)
5. Behley, J., Garbade, M., Milioto, A., Quenzel, J., Behnke, S., Stachniss, C., Gall, J.: Semantickitti: A dataset for semantic scene understanding of lidar sequences. In: Proceedings of the IEEE/CVF International Conference on Computer Vision. pp. 9297–9307 (2019) [1](#), [21](#)
6. Berthelot, D., Carlini, N., Goodfellow, I., Papernot, N., Oliver, A., Raffel, C.A.: Mixmatch: A holistic approach to semi-supervised learning. In: Advances in Neural Information Processing Systems (2019) [2](#), [4](#)
7. Caesar, H., Bankiti, V., Lang, A.H., Vora, S., Liong, V.E., Xu, Q., Krishnan, A., Pan, Y., Baldan, G., Beijbom, O.: nuscenes: A multimodal dataset for autonomous driving. In: Proceedings of the IEEE/CVF Conference on Computer Vision and Pattern Recognition. pp. 11621–11631 (2020) [1](#), [2](#), [3](#), [7](#), [8](#), [13](#), [15](#), [16](#), [18](#), [27](#)
8. Cao, Y., Fang, Z., Wu, Y., Zhou, D.X., Gu, Q.: Towards understanding the spectral bias of deep learning. arXiv preprint arXiv:1912.01198 (2019) [3](#), [7](#), [8](#), [20](#)
9. Chang, M.F., Lambert, J., Sangkloy, P., Singh, J., Bak, S., Hartnett, A., Wang, D., Carr, P., Lucey, S., Ramanan, D., Hays, J.: Argoverse: 3d tracking and forecasting with rich maps. In: Proceedings of the IEEE/CVF Conference on Computer Vision and Pattern Recognition. pp. 8748–8757 (2019) [1](#)
10. Chen, X., Yuan, Y., Zeng, G., Wang, J.: Semi-supervised semantic segmentation with cross pseudo supervision. In: Proceedings of the IEEE/CVF Conference on Computer Vision and Pattern Recognition. pp. 2613–2622 (2021) [9](#), [14](#), [26](#), [28](#), [29](#), [30](#), [31](#), [32](#)
11. Choi, J., Kim, T., Kim, C.: Self-ensembling with gan-based data augmentation for domain adaptation in semantic segmentation. In: Proceedings of the IEEE/CVF International Conference on Computer Vision. pp. 6830–6840 (2019) [4](#)
12. Cordts, M., Omran, M., Ramos, S., Rehfeld, T., Enzweiler, M., Benenson, R., Franke, U., Roth, S., Schiele, B.: The cityscapes dataset for semantic urban scene understanding. In: Proceedings of the IEEE/CVF Conference on Computer Vision and Pattern Recognition. pp. 3213–3223 (2016) [4](#)
13. Cortinhal, T., Tzelepis, G., Aksoy, E.E.: Salsanext: Fast, uncertainty-aware semantic segmentation of lidar point clouds for autonomous driving. arXiv preprint arXiv:2003.03653 (2020) [6](#), [20](#), [21](#)
14. Dai, D., Gool, L.V.: Dark model adaptation: Semantic image segmentation from daytime to nighttime. In: International Conference on Intelligent Transportation Systems. pp. 3819–3824 (2018) [4](#)
15. DeVries, T., Taylor, G.W.: Improved regularization of convolutional neural networks with cutout. arXiv preprint arXiv:1708.04552 (2017) [2](#), [4](#), [11](#), [22](#)

16. Dewan, A., Burgard, W.: Deeptemporalseg: Temporally consistent semantic segmentation of 3d lidar scans. In: IEEE International Conference on Robotics and Automation. pp. 2624–2630 (2020) [21](#)
17. Dong, J., Cong, Y., Sun, G., Liu, Y., Xu, X.: Cscsl: Critical semantic-consistent learning for unsupervised domain adaptation. In: European Conference on Computer Vision. pp. 745–762 (2020) [4](#)
18. Du, L., Tan, J., Yang, H., Feng, J., Xue, X., Zheng, Q., Ye, X., Zhang, X.: Ssf-dan: Separated semantic feature based domain adaptation network for semantic segmentation. In: Proceedings of the IEEE/CVF International Conference on Computer Vision. pp. 982–991 (2019) [4](#)
19. Fong, W.K., Mohan, R., Hurtado, J.V., Zhou, L., Caesar, H., Beijbom, O., Valada, A.: Panoptic nusenes: A large-scale benchmark for lidar panoptic segmentation and tracking. arXiv preprint arXiv:2109.03805 (2021) [1](#)
20. French, G., Laine, S., Aila, T., Mackiewicz, M., Finlayson, G.: Semi-supervised semantic segmentation needs strong, varied perturbations. arXiv preprint arXiv:1906.01916 (2019) [2](#), [22](#)
21. Gan, L., Zhang, R., Grizzle, J.W., Eustice, R.M., Ghaffari, M.: Bayesian spatial kernel smoothing for scalable dense semantic mapping. IEEE Robotics and Automation Letters **5**(2), 790–797 (2020) [21](#)
22. Ganin, Y., Lempitsky, V.: Unsupervised domain adaptation by backpropagation. In: International Conference on Machine Learning. pp. 1180–1189 (2015) [2](#), [4](#)
23. Ganin, Y., Ustinova, E., Ajakan, H., Germain, P., Larochelle, H., Laviolette, F., Marchand, M., Lempitsky, V.: Domain-adversarial training of neural networks. Journal of Machine Learning Research **17**, 1–35 (2016) [2](#), [4](#)
24. Gao, B., Pan, Y., Li, C., Geng, S., Zhao, H.: Are we hungry for 3d lidar data for semantic segmentation? a survey of datasets and methods. IEEE Transactions on Intelligent Transportation Systems (2021) [1](#)
25. Geyer, J., Kassahun, Y., Mahmudi, M., Ricou, X., Durgesh, R., Chung, A.S., Hauswald, L., Pham, V.H., Mühlegg, M., Dorn, S., Fernandez, T., Jänicke, M., Mirashi, S., Savani, C., Sturm, M., Vorobiov, O., Oelker, M., Garreis, S., Schuberth, P.: A2d2: Audi autonomous driving dataset. arXiv preprint arXiv:2004.06320 (2020) [1](#)
26. Goodfellow, I., Pouget-Abadie, J., Mirza, M., Xu, B., Warde-Farley, D., Ozair, S., Courville, A., Bengio, Y.: Generative adversarial nets. In: Advances in Neural Information Processing Systems. pp. 2672–2680 (2014) [2](#), [4](#)
27. Grandvalet, Y., Bengio, Y.: Semi-supervised learning by entropy minimization. In: Proceedings of the International Conference on Neural Information Processing Systems. pp. 529–536 (2004) [3](#), [5](#)
28. He, K., Zhang, X., Ren, S., Sun, J.: Deep residual learning for image recognition. In: Proceedings of the IEEE/CVF Conference on Computer Vision and Pattern Recognition. pp. 770–778 (2016) [6](#), [20](#)
29. Hoffman, J., Tzeng, E., Park, T., Zhu, J.Y., Isola, P., Saenko, K., Efros, A., Darrell, T.: Cycada: Cycle-consistent adversarial domain adaptation. In: International Conference on Machine Learning. pp. 1989–1998 (2015) [4](#)
30. Houston, J., Zuidhof, G., Bergamini, L., Ye, Y., Chen, L., Jain, A., Omari, S., Igloukov, V., Ondruska, P.: One thousand and one hours: Self-driving motion prediction dataset. arXiv preprint arXiv:2006.14480 (2020) [1](#)
31. Hu, Q., Yang, B., Xie, L., Rosa, S., Guo, Y., Wang, Z., Trigoni, N., Markham, A.: Randla-net: Efficient semantic segmentation of large-scale point clouds. In: Proceedings of the IEEE/CVF Conference on Computer Vision and Pattern Recognition. pp. 11108–11117 (2020) [21](#)

32. Jaritz, M., Vu, T.H., de Charette, R., Wirbel, E., Pérez, P.: xmuda: Cross-modal unsupervised domain adaptation for 3d semantic segmentation. In: Proceedings of the IEEE/CVF Conference on Computer Vision and Pattern Recognition. pp. 12605–12614 (2020) [4](#), [9](#), [13](#)
33. Jiang, P., Saripalli, S.: Lidarnet: A boundary-aware domain adaptation model for point cloud semantic segmentation. In: IEEE International Conference on Robotics and Automation. pp. 2457–2464 (2021) [4](#)
34. Kim, M., Byun, H.: Learning texture invariant representation for domain adaptation of semantic segmentation. In: Proceedings of the IEEE/CVF Conference on Computer Vision and Pattern Recognition. pp. 12975–12984 (2020) [4](#)
35. Landrieu, L., Simonovsky, M.: Large-scale point cloud semantic segmentation with superpoint graphs. In: Proceedings of the IEEE/CVF Conference on Computer Vision and Pattern Recognition. pp. 4558–4567 (2018) [21](#)
36. Lee, D.H.: Pseudo-label: The simple and efficient semi-supervised learning method for deep neural networks. In: International Conference on Machine Learning Workshop. pp. 896–901 (2013) [2](#), [4](#), [6](#)
37. Li, Y., Ibanez-Guzman, J.: Lidar for autonomous driving: The principles, challenges, and trends for automotive lidar and perception systems. IEEE Signal Processing Magazine **37**(4), 50–61 (2020) [1](#)
38. Li, Y., Yuan, L., Vasconcelos, N.: Bidirectional learning for domain adaptation of semantic segmentation. In: Proceedings of the IEEE/CVF Conference on Computer Vision and Pattern Recognition. pp. 6936–6945 (2019) [4](#), [9](#), [12](#), [13](#)
39. Long, J., Shelhamer, E., Darrell, T.: Fully convolutional networks for semantic segmentation. In: Proceedings of the IEEE/CVF Conference on Computer Vision and Pattern Recognition. pp. 3431–3440 (2015) [6](#), [20](#)
40. Loshchilov, I., Hutter, F.: Decoupled weight decay regularization. In: International Conference on Learning Representations (2018) [9](#)
41. Luo, Y., Zheng, L., Guan, T., Yu, J., Yang, Y.: Taking a closer look at domain shift: Category-level adversaries for semantics consistent domain adaptation. In: Proceedings of the IEEE/CVF Conference on Computer Vision and Pattern Recognition. pp. 2507–2516 (2019) [4](#)
42. Luo, Y., Zhu, J., Li, M., Ren, Y., Zhang, B.: Smooth neighbors on teacher graphs for semi-supervised learning. In: Proceedings of the IEEE/CVF Conference on Computer Vision and Pattern Recognition. pp. 8896–8905 (2018) [2](#)
43. Luo, Z., Cai, Z., Zhou, C., Zhang, G., Zhao, H., Yi, S., Lu, S., Li, H., Zhang, S., Liu, Z.: Unsupervised domain adaptive 3d detection with multi-level consistency. In: Proceedings of the IEEE/CVF International Conference on Computer Vision. pp. 8866–8875 (2021) [4](#)
44. Ma, H., Lin, X., Wu, Z., Yu, Y.: Coarse-to-fine domain adaptive semantic segmentation with photometric alignment and category-center regularization. In: Proceedings of the IEEE/CVF Conference on Computer Vision and Pattern Recognition. pp. 4051–4060 (2021) [4](#)
45. Mei, K., Zhu, C., Zou, J., Zhang, S.: Instance adaptive self-training for unsupervised domain adaptation. In: European Conference on Computer Vision. pp. 415–430 (2020) [4](#)
46. Milioto, A., Vizzo, I., Behley, J., Stachniss, C.: Rangenet++: Fast and accurate lidar semantic segmentation. In: IEEE/RSJ International Conference on Intelligent Robots and Systems. pp. 4213–4220 (2019) [6](#), [20](#), [21](#)
47. Neuhold, G., Ollmann, T., Bulow, S.R., Kotschieder, P.: The mapillary vistas dataset for semantic understanding of street scenes. In: Proceedings of the

- IEEE/CVF International Conference on Computer Vision. pp. 4990–4999 (2017) [4](#)
48. Olsson, V., Tranheden, W., Pinto, J., Svensson, L.: Classmix: Segmentation-based data augmentation for semi-supervised learning. In: Proceedings of the IEEE/CVF Winter Conference on Applications of Computer Vision. pp. 1369–1378 (2021) [4](#)
 49. Ouali, Y., Hudelot, C., Tami, M.: An overview of deep semi-supervised learning. arXiv preprint arXiv:2006.05278 (2020) [22](#)
 50. Pan, F., Shin, I., Rameau, F., Lee, S., Kweon, I.S.: Unsupervised intra-domain adaptation for semantic segmentation through self-supervision. In: Proceedings of the IEEE/CVF Conference on Computer Vision and Pattern Recognition. pp. 3764–3773 (2020) [3](#), [4](#), [5](#), [9](#), [12](#), [13](#), [23](#)
 51. Pan, S.J., Yang, Q.: A survey on transfer learning. *IEEE Transactions on Knowledge and Data Engineering* **22**(10), 1345–1359 (2009) [1](#)
 52. Peng, D., Lei, Y., Li, W., Zhang, P., Guo, Y.: Sparse-to-dense feature matching: Intra and inter domain cross-modal learning in domain adaptation for 3d semantic segmentation. In: Proceedings of the IEEE/CVF International Conference on Computer Vision. pp. 7108–7117 (2021) [4](#)
 53. Qi, C.R., Su, H., Mo, K., Guibas, L.J.: Pointnet: Deep learning on point sets for 3d classification and segmentation. In: Proceedings of the IEEE/CVF Conference on Computer Vision and Pattern Recognition. pp. 652–660 (2017) [21](#)
 54. Qi, C.R., Yi, L., Su, H., Guibas, L.J.: Pointnet++: Deep hierarchical feature learning on point sets in a metric space. In: Advances in Neural Information Processing Systems (2017) [21](#)
 55. Radford, A., Metz, L., Chintala, S.: Unsupervised representation learning with deep convolutional generative adversarial networks. arXiv preprint arXiv:1511.06434 (2015) [4](#)
 56. Ramamonjison, R., Banitalebi-Dehkordi, A., Kang, X., Bai, X., Zhang, Y.: Simrod: A simple adaptation method for robust object detection. In: Proceedings of the IEEE/CVF International Conference on Computer Vision. pp. 3570–3579 (2021) [4](#), [11](#), [22](#)
 57. Richter, S.R., Vineet, V., Roth, S., Koltun, V.: Playing for data: Ground truth from computer games. In: European Conference on Computer Vision. pp. 102–118 (2016) [4](#)
 58. Ros, G., Sellart, L., Materzynska, J., Vazquez, D., Lopez, A.M.: The synthia dataset: A large collection of synthetic images for semantic segmentation of urban scenes. In: Proceedings of the IEEE/CVF Conference on Computer Vision and Pattern Recognition. pp. 3234–3243 (2016) [4](#)
 59. Rosu, R.A., Schütt, P., Quenzel, J., Behnke, S.: Latticenet: Fast point cloud segmentation using permutohedral lattices. arXiv preprint arXiv:1912.05905 (2019) [21](#)
 60. Sahoo, A., Panda, R., Feris, R., Saenko, K., Das, A.: Select, label, and mix: Learning discriminative invariant feature representations for partial domain adaptation. arXiv preprint arXiv:2012.03358 (2020) [4](#)
 61. Sakaridis, C., Dai, D., Gool, L.V.: Acdc: The adverse conditions dataset with correspondences for semantic driving scene understanding. arXiv preprint arXiv:2104.13395 (2021) [4](#)
 62. Shannon, C.E.: A mathematical theory of communication. *the Bell System Technical Journal* **27**(3), 379–423 (1948) [3](#)
 63. Sinha, S., Garg, A., Larochelle, H.: Curriculum by smoothing. arXiv preprint arXiv:2003.01367 (2020) [3](#), [7](#), [8](#), [20](#)

64. Smith, L.N., Topin, N.: Super-convergence: Very fast training of neural networks using large learning rates. arXiv preprint arXiv:1708.07120 (2017) **9**
65. Su, H., Jampani, V., Sun, D., Maji, S., Kalogerakis, E., Yang, M.H., Kautz, J.: Splatnet: Sparse lattice networks for point cloud processing. In: Proceedings of the IEEE/CVF Conference on Computer Vision and Pattern Recognition. pp. 2530–2539. (2018) **21**
66. Sun, P., Kretzschmar, H., Dotiwalla, X., Chouard, A., Patnaik, V., Tsui, P., Guo, J., Chai, Y.Z.Y., Caine, B., Vasudevan, V., Han, W., Ngiam, J., Zhao, H., Timofeev, A., Ettinger, S., Krivokon, M., Gao, A., Joshi, A., Zhang, Y., Shlens, J., Chen, Z., Anguelov, D.: Scalability in perception for autonomous driving: Waymo open dataset. In: Proceedings of the IEEE/CVF Conference on Computer Vision and Pattern Recognition. pp. 2446–2454 (2020) **1**
67. Tarvainen, A., Valpola, H.: Mean teachers are better role models: Weight-averaged consistency targets improve semi-supervised deep learning results. In: Advances in Neural Information Processing Systems (2017) **9, 14, 26, 28, 29, 30, 31, 32**
68. Tatarchenko, M., Park, J., Koltun, V., Zhou, Q.Y.: Tangent convolutions for dense prediction in 3d. In: Proceedings of the IEEE/CVF Conference on Computer Vision and Pattern Recognition. pp. 3887–3896 (2018) **21**
69. Toldo, M., Maracani, A., Michieli, U., Zanuttigh, P.: Unsupervised domain adaptation in semantic segmentation: A review. Technologies **8**(2), 1–35 (2020) **2**
70. Tranheden, W., Olsson, V., Pinto, J., Svensson, L.: Dacs: Domain adaptation via cross-domain mixed sampling. In: Proceedings of the IEEE/CVF Winter Conference on Applications of Computer Vision. pp. 1379–1389 (2021) **4**
71. Triess, L.T., Dreissig, M., Rist, C.B., Zöllner, J.M.: A survey on deep domain adaptation for lidar perception. arXiv preprint arXiv:2106.02377 (2021) **4**
72. Tsai, Y.H., Hung, W.C., Schuster, S., Sohn, K., Yang, M.H., Chandraker, M.: Learning to adapt structured output space for semantic segmentation. In: Proceedings of the IEEE/CVF Conference on Computer Vision and Pattern Recognition. pp. 7472–7481 (2018) **4, 9, 12, 13, 14, 26, 28, 29, 30, 31, 32**
73. Vasconcelos, C., Larochelle, H., Dumoulin, V., Romijnders, R., Roux, N.L., Goroshin, R.: Impact of aliasing on generalization in deep convolutional networks. In: Proceedings of the IEEE/CVF International Conference on Computer Vision. pp. 10529–10538 (2021) **3, 4, 7, 8, 21**
74. Verma, V., Kawaguchi, K., Lamb, A., Kannala, J., Solin, A., Bengio, Y., Lopez-Paz, D.: Interpolation consistency training for semi-supervised learning. Neural Networks (2021) **2, 4**
75. Vu, T.H., Jain, H., Bucher, M., Cord, M., Pérez, P.: Advent: Adversarial entropy minimization for domain adaptation in semantic segmentation. In: Proceedings of the IEEE/CVF Conference on Computer Vision and Pattern Recognition. pp. 2517–2526 (2019) **3, 4, 9, 12, 13, 14, 26, 28, 29, 30, 31, 32**
76. Vu, T.H., Jain, H., Bucher, M., Cord, M., Pérez, P.: Dada: Depth-aware domain adaptation in semantic segmentation. In: Proceedings of the IEEE/CVF International Conference on Computer Vision. pp. 7364–7373 (2019) **4, 9, 12, 13, 14, 23, 26, 28, 29, 30, 31, 32**
77. Wang, H., Shen, T., Zhang, W., Duan, L.Y., Mei, T.: Classes matter: A fine-grained adversarial approach to cross-domain semantic segmentation. In: European Conference on Computer Vision. pp. 642–659 (2020) **4**
78. Wang, Y., Peng, J., Zhang, Z.: Uncertainty-aware pseudo label refinery for domain adaptive semantic segmentation. In: Proceedings of the IEEE/CVF International Conference on Computer Vision. pp. 9092–9101 (2021) **3, 5, 8**

79. Wang, Z., Yu, M., Wei, Y., Feris, R., Xiong, J., mei Hwu, W., Huang, T.S., Shi, H.: Differential treatment for stuff and things: A simple unsupervised domain adaptation method for semantic segmentation. In: Proceedings of the IEEE/CVF Conference on Computer Vision and Pattern Recognition. pp. 12635–12644 (2020) [4](#)
80. Wu, B., Wan, A., Yue, X., Keutzer, K.: Squeezeseg: Convolutional neural nets with recurrent crf for real-time road-object segmentation from 3d lidar point cloud. In: IEEE International Conference on Robotics and Automation. pp. 1887–1893 (2018) [21](#)
81. Wu, B., Zhou, X., Zhao, S., Yue, X., Keutzer, K.: Squeezesegv2: Improved model structure and unsupervised domain adaptation for road-object segmentation from a lidar point cloud. In: IEEE International Conference on Robotics and Automation. pp. 4376–4382 (2019) [6](#), [21](#)
82. Wu, Z., Han, X., Lin, Y.L., Uzunbas, M.G., Goldstein, T., Lim, S.N., Davis, L.S.: Dcan: Dual channel-wise alignment networks for unsupervised scene adaptation. In: European Conference on Computer Vision. pp. 518–534 (2018) [4](#)
83. Xu, C., Wu, B., Wang, Z., Zhan, W., Vajda, P., Keutzer, K., Tomizuka, M.: Squeezesegv3: Spatially-adaptive convolution for efficient point-cloud segmentation. In: European Conference on Computer Vision. pp. 1–19 (2020) [6](#), [21](#)
84. Xu, M., Zhang, J., Ni, B., Li, T., Wang, C., Tian, Q., Zhang, W.: Adversarial domain adaptation with domain mixup. In: Proceedings of the AAAI Conference on Artificial Intelligence. pp. 6502–6509 (2020) [4](#)
85. Yang, J., An, W., Wang, S., Zhu, X., Yan, C., Huang, J.: Label-driven reconstruction for domain adaptation in semantic segmentation. In: European Conference on Computer Vision. pp. 480–498 (2020) [4](#)
86. Yang, Y., Soatto, S.: Fda: Fourier domain adaptation for semantic segmentation. In: Proceedings of the IEEE/CVF Conference on Computer Vision and Pattern Recognition. pp. 4085–4095 (2020) [4](#)
87. Yi, L., Gong, B., Funkhouser, T.: Complete & label: A domain adaptation approach to semantic segmentation of lidar point clouds. In: Proceedings of the IEEE/CVF Conference on Computer Vision and Pattern Recognition. pp. 15363–15373 (2021) [4](#)
88. Yu, F., Chen, H., Wang, X., Xian, W., Chen, Y., Liu, F., Madhavan, V., Darrell, T.: Bdd100k: A diverse driving dataset for heterogeneous multitask learning. In: Proceedings of the IEEE/CVF Conference on Computer Vision and Pattern Recognition. pp. 2636–2645 (2020) [4](#)
89. Yuan, J., Liu, Y., Shen, C., Wang, Z., Li, H.: A simple baseline for semi-supervised semantic segmentation with strong data augmentation. In: Proceedings of the IEEE/CVF International Conference on Computer Vision. pp. 8229–8238 (2021) [22](#)
90. Yue, X., Wu, B., Seshia, S.A., Keutzer, K., Sangiovanni-Vincentelli, A.L.: A lidar point cloud generator: From a virtual world to autonomous driving. In: ACM International Conference on Multimedia Retrieval. pp. 458–464 (2018) [1](#)
91. Yun, S., Han, D., Oh, S.J., Chun, S., Choe, J., Yoo, Y.: Cutmix: Regularization strategy to train strong classifiers with localizable features. In: Proceedings of the IEEE/CVF International Conference on Computer Vision. pp. 6023–6032 (2019) [2](#), [4](#), [11](#), [22](#)
92. Zhang, H., Cisse, M., Dauphin, Y.N., Lopez-Paz, D.: mixup: Beyond empirical risk minimization. In: International Conference on Learning Representations (2018) [2](#), [4](#), [11](#), [22](#)

93. Zhang, R.: Making convolutional networks shift-invariant again. In: International Conference on Machine Learning. pp. 7324–7334 (2019) [3](#), [4](#), [7](#), [21](#)
94. Zhang, Y., Zhou, Z., David, P., Yue, X., Xi, Z., Gong, B., Foroosh, H.: Polarnet: An improved grid representation for online lidar point clouds semantic segmentation. In: Proceedings of the IEEE/CVF Conference on Computer Vision and Pattern Recognition. pp. 9601–9610 (2020) [21](#)
95. Zhao, S., Wang, Y., Li, B., Wu, B., Gao, Y., Xu, P., Darrell, T., Keutze, K.: epointda: An end-to-end simulation-to-real domain adaptation framework for lidar point cloud segmentation. arXiv preprint arXiv:2009.03456 (2020) [4](#)
96. Zhao, Y., Bai, L., Huang, X.: Fidnet: Lidar point cloud semantic segmentation with fully interpolation decoding. In: IEEE/RSJ International Conference on Intelligent Robots and Systems. pp. 4453–4458 (2021) [21](#)
97. Zheng, Z., Yang, Y.: Unsupervised scene adaptation with memory regularization in vivo. In: International Joint Conference on Artificial Intelligence. pp. 1076–1082 (2020) [3](#), [4](#)
98. Zoph, B., Ghiasi, G., Lin, T.Y., Cui, Y., Liu, H., Cubuk, E.D., Le, Q.V.: Rethinking pre-training and self-training. In: Advances in Neural Information Processing Systems (2020) [2](#), [4](#)
99. Zou, X., Xiao, F., Yu, Z., Lee, Y.J.: Delving deeper into anti-aliasing in convnets. In: British Machine Vision Conference (2020) [3](#), [4](#), [7](#), [21](#)
100. Zou, Y., Yu, Z., Kumar, B.V.K., Wang, J.: Unsupervised domain adaptation for semantic segmentation via class-balanced self-training. In: European Conference on Computer Vision. pp. 289–305 (2018) [2](#), [4](#), [7](#), [9](#), [12](#), [13](#), [14](#), [23](#), [26](#), [28](#), [29](#), [30](#)
101. Zou, Y., Yu, Z., Liu, X., Kumar, B.V.K., Wang, J.: Confidence regularized self-training. In: Proceedings of the IEEE/CVF International Conference on Computer Vision. pp. 5982–5991 (2019) [4](#), [7](#)

Acknowledgements. We thank Sergi Widjaja, Xiaogang Wang, Dhananjai Sharma, and Edouard Francois Marc Capellier for their insightful reviews and discussions.